HHS Public Access

Author manuscript

Cell Metab. Author manuscript; available in PMC 2022 July 06.

Published in final edited form as:

Cell Metab. 2021 July 06; 33(7): 1404–1417.e9. doi:10.1016/j.cmet.2021.05.003.

Brain glycogen serves as a critical glucosamine cache required for protein glycosylation

Ramon C. Sun[1,3,*], **Lyndsay E.A. Young**[2,3], **Ronald C. Bruntz**[2], **Kia H. Markussen**[2], **Zhengqiu Zhou**[2], **Lindsey R. Conroy**[1,3], **Tara R. Hawkinson**[1], **Harrison A. Clarke**[1], **Alexandra E. Stanback**[1], **Jessica K.A. Macedo**[2], **Shane Emanuelle**[2], **M. Kathryn Brewer**[2,4], **Alberto L. Rondon**[2], **Annette Mestas**[2], **William C. Sanders**[2], **Krishna K. Mahalingan**[5], **Buyun Tang**[5], **Vimbai M. Chikwana**[5], **Dyann M. Segvich**[5], **Christopher J. Contreras**[5], **Elizabeth J. Allenger**[6], **Christine F. Brainson**[7], **Lance A. Johnson**[6], **Richard E. Taylor**[8], **Dustin D. Armstrong**[9], **Robert Shaffer**[10], **Charles J. Waechter**[2], **Craig W. Vander Kooi**[2,3], **Anna A. DePaoli-Roach**[5], **Peter J. Roach**[5], **Thomas D. Hurley**[5], **Richard R. Drake**[11], **Matthew S. Gentry**[2,3,*,#]

[1]Department of Neuroscience, University of Kentucky, Lexington, Kentucky, USA

[2]Department of Molecular and Cellular Biochemistry, University of Kentucky, Lexington, Kentucky, USA

[3]Markey Cancer Center, University of Kentucky, Lexington, Kentucky, USA

[4]Institute for Research in Biomedicine, Barcelona, Spain

[5]Biochemistry and Molecular Biology, Indiana University School of Medicine, Indianapolis, Indiana, USA

[6]Department of Physiology, University of Kentucky, Lexington, Kentucky, USA

[7]Department of Toxicology and Cancer Biology, University of Kentucky, Lexington, Kentucky, USA

[8]Department of Chemistry & Biochemistry and the Warren Center for Drug Discovery, University of Notre Dame, Notre Dame, Indiana, USA

[9]Parasail LLC, Boston, Massachusetts, USA

[10]Enable Therapeutics, Boston, Massachusetts, USA

[*]Correspondence: ramon.sun@uky.edu, matthew.gentry@uky.edu.
[#]Lead Contact

Author Contributions

Conceptualization, R.C.S. and M.S.G.; Methodology, R.C.S., M.S.G., and R.R.D.; Investigation, R.C.S, L.E.A.Y, A.E.S., R.C.B., K.H.M., Z.Q.Z., J.K.A.M., S.E., M.K.B., A.L.R., W.C.S., K.K.M., B.T., V.M.C., D.M.S., C.J.C., E.J.A., C.F.B., L.A.J., R.E.T., C.W.V.K., C.W., A.A.D.R., P.J.R., T.D.H., L.R.C., and R.R.D.; Writing – Original Draft, R.C.S. and M.S.G.; Writing – Review & Editing, R.C.S. C.W.V.K., A.A.D.R., P.J.R., and M.S.G.; Funding Acquisition, R.C.S. and M.S.G.; Resources, R.C.S. and M.S.G.; Supervision, R.C.S. and M.S.G.

Declaration of Interests: M.S.G. is a consultant for Maze Therapeutics, Enable Therapeutics, Glut1-Deficiency Syndrome Foundation, and Chelsea's Hope. M.S.G., R.C.S., C.W.V.K., and R.C.B. are founders of Atterogen, LLC.

[11]Cell and Molecular Pharmacology and Experimental Therapeutics, Medical University of South Carolina, Charleston, South Carolina, USA

Summary

Glycosylation defects are a hallmark of many nervous system diseases. However, the molecular and metabolic basis for this pathology are not fully understood. In this study, we found that N-linked protein glycosylation in the brain is metabolically channelled to glucosamine metabolism through glycogenolysis. We discovered that glucosamine is an abundant constituent of brain glycogen, which functions as a glucosamine reservoir for multiple glycoconjugates. We demonstrated the enzymatic incorporation of glucosamine into glycogen by glycogen synthase, and the release by glycogen phosphorylase by biochemical and structural methodologies, in primary astrocytes, and *in vivo* by isotopic tracing and mass spectrometry. Using two mouse models of glycogen storage diseases, we showed that disruption of brain glycogen metabolism causes global decreases in free pools of UDP-N-acetylglucosamine and N-linked protein glycosylation. These findings revealed fundamental biological roles for brain glycogen in protein glycosylation with direct relevance to multiple human diseases of the central nervous system.

Graphical Abstract

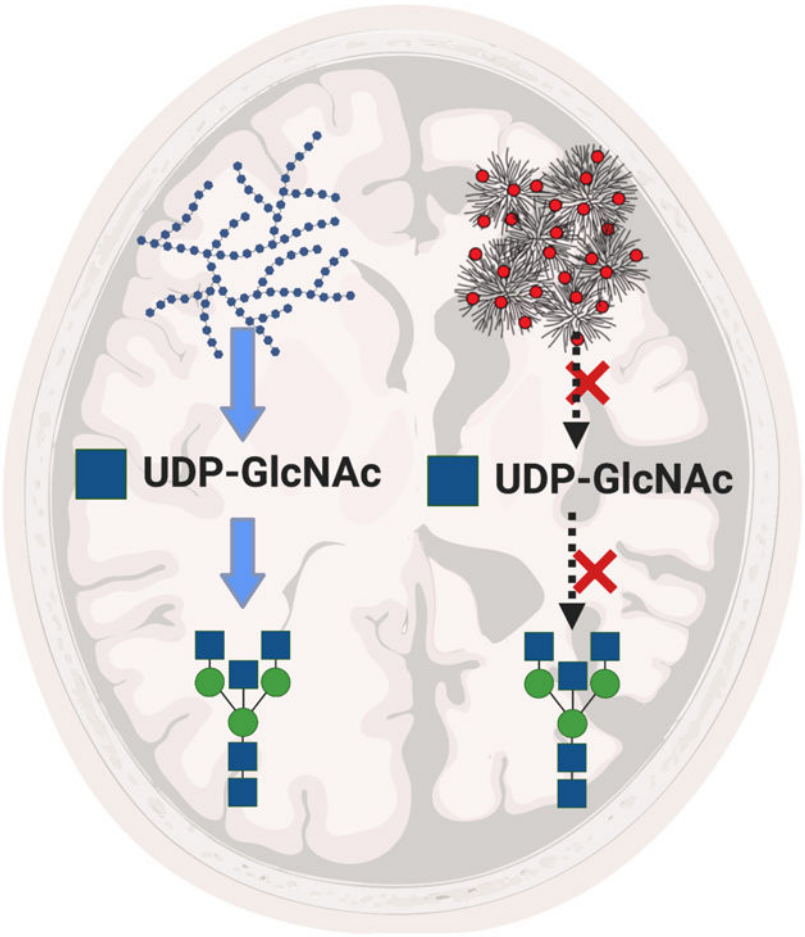

eTOC blurb:

Sun et al. demonstrate that glycogen serves as a critical reservoir of glucosamine in the nervous system and map protein N-glycosylation patterns in the brain. In models of glycogen storage diseases, impaired flux of glucosamine through glycogen, by the same enzymes that mediate flux of glucose, is associated with reduced protein N-glycosylation.

Introduction

Glycosylation is one of the most abundant and complex co-translational and posttranslational modifications of proteins affecting multiple biological processes, including protein folding, maturation, stability, subcellular localization, enzymatic activity, and protein-protein interactions (Schwarz and Aebi, 2011). The biological relevance and diversity of glycosylation is evidenced by the prediction that 2% of human genes participate in glycan metabolism or regulation and by the existence of more than 125 human disorders linked to mutations in those genes (Narimatsu et al., 2019; Ng and Freeze, 2018). Moreover, primary symptoms of congenital disorders of glycosylation (CDGs) are neurological, including seizures, delayed intellectual development, cognitive impairment, and cerebellar hypoplasia (Freeze et al., 2015). These phenotypes are not surprising because the process of N-linked glycosylation is important in modulating synaptic plasticity, neurite outgrowth and neuron morphology, and many cognitive processes, such as learning and memory formation (Benson et al., 2000; Kleene and Schachner, 2004; Wasser et al., 2014). Furthermore, aberrant N-linked glycosylation results in neuroinflammation, neuronal cell death, and gliosis (Patterson, 2015). Despite these critical functions, many molecular aspects of brain-specific N-glycan metabolism remain unresolved, hindering a fundamental understanding of the biology, disease, and discovery of novel therapeutics for neurological disorders.

Glycogen is the storage polysaccharide in animals and plays pivotal roles in brain metabolism (Brewer and Gentry, 2019). On a molecular level, glycogen is a metabolic substrate for neuronal lactate release, ATP production, and GABA biosynthesis on a cellular level. Glycogen metabolism contributes to locomotion (Sinadinos et al., 2014), memory formation (Duran et al., 2013) and life span (Gusarov et al., 2017). The importance of brain glycogen is highlighted by its role in inherited disease. For example, Lafora disease (LD) is a glycogen storage disease (GSD) that impacts the brain (Gentry et al., 2018). Large insoluble, aberrant glycogen aggregates called polyglucosan bodies (PGBs), or Lafora bodies in the context of LD, accumulate in astrocytes and neurons of the patients and drive rapid cognitive decline, myoclonus, and epileptic seizures (Gentry et al., 2018; Nitschke et al., 2018). PGB accumulation is also associated with aging and dementia (Duran et al., 2019; Johnson et al., 2020). Studies suggest a link between PGB accumulation and aberrant glycosylation in the brain (Iwaki et al., 1996; Kimura et al., 1998; Ondruskova et al., 2014), indicating that glycogen and N-glycans are metabolically intertwined. However, the molecular connection and biological implications are unknown.

Brain PGBs are primarily comprised of glucose (Sakai et al., 1969; Stam and Roukema, 1973), but they react with lectins specific for N-acetylglucosamine (GlcNAc), galactose, and fucose (Nishimura et al., 2000). Herein, we discovered that glucosamine accounts for up to

25% of covalently linked sugar monomers in brain glycogen. Using isotopic tracer mass spectrometry, enzymology, and structural biology, we found that the enzymatic incorporation into and release of glucosamine from glycogen in the brain are mediated by glycogen synthase (GYS) and glycogen phosphorylase (GP), respectively. We show the importance of this metabolic pathway in two distinct mouse models of neurological GSDs. In both diseases, brain PGBs sequestered glucosamine, thereby decreasing glucosamine pools and limiting the production of UDP-GlcNAc, the fundamental building block of N-glycans. Utilizing matrix-assisted laser desorption/ionization traveling-wave ion-mobility high-resolution mass spectrometry (MALDI TW IMS), we developed a novel mass spectrometry imaging method to quantify and spatially visualize glycogen and N-glycan abundance *in situ*. Our data indicate that abnormal glycogen accumulation in GSDs impairs the release of glucosamine from glycogen and consequently compromises N-glycan production in the brain. These data demonstrate that glycogen is more than a glucose cache; it is also a critical storage macromolecule for brain protein N-glycosylation, which impacts myriad subsequent cellular processes.

Results

Glucosamine incorporation into glycogen by glycogen synthase

Intriguing reports from the 1980s suggested that liver glycogen contains covalent monosaccharides other than glucose, specifically glucosamine (Kirkman et al., 1989; Kirkman and Whelan, 1986). However, the biological relevance of this observation was not explored, and glycogen from multiple tissues was not examined. Therefore, we purified glycogen from multiple mouse tissues using centrifugation and sucrose gradients, followed by dialysis to remove noncovalently linked sugars (Roe et al., 1961; Young et al., 2020). The purified glycogen was then treated with mild acid to hydrolyze glycosidic bonds (Young et al., 2020), and the monomeric composition of the sugars were analyzed by gas chromatography-mass spectrometry (GCMS) (Figure 1A). We detected glucosamine in both liver and muscle glycogen at similar amounts as previously reported (Kirkman et al., 1989; Kirkman and Whelan, 1986). Muscle glycogen contained 1% glucosamine and liver glycogen contained 0.1% (Figures 1B-C, S1A-D). Strikingly, brain glycogen contained 25% glucosamine (Figures 1B-C, S1A-D). The final wash and undigested glycogen were analyzed as controls, and no noncovalent glucosamine was identified in either fraction (Figure S1E).

Direct uptake and utilization of glucosamine is well-established in the mammalian brain (Harpur and Quastel, 1949; Tan et al., 1977b). Glucosamine directly crosses the blood-brain-barrier (Popov, 1985) and accumulates in synaptosomes (Tan et al., 1977a) and ganglions (Bennett et al., 1973) for the production of gangliosides (Liepkalns et al., 1983) and glycoproteins (Holian et al., 1971; Ramirez, 1974). We hypothesized that a portion of glucosamine is sequestered in glycogen. To test if glucosamine is incorporated into glycogen *in situ*, we incubated primary astrocytes in media enriched with 2 mM $^{13}C_6$-glucosamine and quantified labeled glycogen. After the addition of $^{13}C_6$-glucosamine, metabolism was quenched at multiple timepoints, glycogen was extracted, and ^{13}C-labeled glucosamine incorporation into glycogen was quantified by GCMS (Figure 1D). We detected a time-

dependent increase of $^{13}C_6$-glucosamine into glycogen over 8 hours (Figure 1D). Surprisingly, maximal $^{13}C_6$-glucosamine incorporation into glycogen was only ~20% of the glycogen-bound glucosamine observed in primary astrocytes (Figure 1D), suggesting an alternative source of intracellular glucosamine. Nutrient exchange to the brain is tightly controlled by the blood brain barrier. Since the primary metabolic fuel for the brain is glucose and glucose is a known precursor for glucosamine (McClain et al., 1992), we hypothesized that glucosamine synthesized from glucose could account for the unlabeled pool of intracellular pool of glucosamine. Using $^{13}C_6$-glucose as a tracer, we observed robust and near complete synthesis of both free and glycogen associated $^{13}C_6$-glucosamine in primary astrocytes quantified by mass spectroscopy (Figure 1F, S1F-I). To confirm glucose as a primary physiological source of brain glucosamine, WT mice were fed a liquid diet enriched with $^{13}C_6$-glucose followed by brain harvesting and mass spectrometry analysis according to established methods (Figure S1G) (Sun et al., 2017). Similar to primary astrocytes, we found significant enrichment of both free and glycogen-bound ^{13}C-glucosamine in the mouse brains at a level comparable to ^{13}C-glucose enrichment in glycogen (Figure S1I). These data support the notion that brain primarily utilizes *de novo* synthesized glucosamine for glycogen incorporation.

The glycogen proteome has been reported in multiple studies (Stapleton et al., 2013; Stapleton et al., 2010), and the only known enzyme for the direct biosynthesis is GYS, which is conserved from yeast to mammals (Baskaran et al., 2011; Buschiazzo et al., 2004). For the incorporation of glucose into glycogen, GYS binds to the carrier molecule UDP-glucose and adds glucose to glycogen while releasing UDP. To determine if UDP-glucosamine is a substrate for GYS, we developed an *in vitro* assay using recombinant yeast Gys2 (yGys2), UDP-glucose or UDP-glucosamine, and the seven-unit dextran polymer maltoheptaose (DP7) as the acceptor. The transfer of either glucose or glucosamine to DP7 from the respective sugar nucleotides was directly assessed by matrix-assisted laser desorption ionization coupled high-definition mass spectrometry (HDMS), which differentiates glucose versus glucosamine due to their 1 *m/z* mass difference (Figure 2A, S2A). Using UDP-glucose or UDP-glucosamine as substrates, yGys2 transferred glucose or glucosamine, respectively, to DP7 and released free UDP as an end product (Figure 2A, S2A). Using this assay, we assessed the rate of glucose or glucosamine incorporation over 360 min. The rate of incorporation reached steady state at ~60 min for either UDP-glucosamine or UDP-glucose as single substrates (Figure 2B, S2B). In the presence of equal amount of both UDP-glucose (1mM) and UDP-glucosamine (1mM), we observed a decreased, but steady rate of glucosamine incorporation (Figure 2B). These data suggest that UDP-glucose and UDP-glucosamine are competitive substrates. Additional competitive assays using multiple sugar donors further supported that UDP-glucosamine is a competitive substrate for yGys2 (Figure S2C-D).

To visualize the interaction between UDP-glucosamine and yGys2, we co-crystallized yGys2 with UDP-glucosamine. The structure of yGys2 bound to UDP-glucosamine was determined at a resolution of 2.98 Å (Figure 2C, S2E, Table S1). The structure revealed yGys2 formed a catalytically poised complex with UDP-glucosamine (Figure 2C). The overall subunit-ligand interactions of UDP-glucosamine were similar to those with UDP-glucose (Chikwana et al., 2013) with the 2'-substituent of the sugar moiety interacting with

the sidechain of Arg199 and the β-phosphate of UDP (Figure 2C). Importantly, the structure had the amine group of glucosamine in the yGys2 active site. Cumulatively, these data provided a mechanism for the direct incorporation of glucosamine into glycogen by GYS.

Glucosamine phosphate release by glycogen phosphorylase

Because our data indicated that glucosamine is incorporated into glycogen by glycogen synthase, we hypothesized that the physiological glycogenolysis of glucosamine occurs through GP. To test this hypothesis, we isolated primary astrocytes from wild-type mice and knocked down the brain GP isoform (*Pygb*) (Figures 3A). PYGB-deficient astrocytes had increased glycogen-derived glucose and glycogen-derived glucosamine (as determined by GCMS of hydrolyzed glycogen) (Figure 3B). We performed a pulse-chase experiment with primary astrocytes grown in the presence of ^{13}C-glucose and then exposed to DMSO (control) or 1,4-dideoxy-1,4-imino-D-arabinitol (DAB), a well-defined GP inhibitor (Fosgerau et al., 2000), in the presence of ^{12}C-glucose. By monitoring the replacement of ^{13}C-glucosamine and ^{13}C-glucose by their ^{12}C-equivalents in purified glycogen, we determined that DAB decreased the replacement of both ^{13}C-glucosamine (Figure 3C) and ^{13}C-glucose (Figure S3A), consistent with GP mediating release of these components from glycogen. To evaluate the direct removal of glucosamine from glycogen by GP, we performed cell-free assays using recombinant PYGB, glycogen debranching enzyme (GDE), and purified mouse brain glycogen and assessed released glucosamine by GCMS (Figure 3D, E). GDE and PYGB are both required for the continuous release of glucose 1-phosphate from glycogen (Adeva-Andany et al., 2016). Neither PYGB nor GDE alone efficiently released glucosamine 1-phosphate from glycogen (Figure 3F). However, reactions with both GDE and PYGB released glucosamine 1-phosphate (Gn1P) from brain glycogen (Figure 3F, S3B-C).

These results for GP and for GYS suggested that glucosamine flux through glycogen occurs through the canonical glycogen metabolic enzymes. GYS incorporated glucosamine into glycogen using UDP-glucosamine as the substrate, and GP released glucosamine in the form of Gn1P from glycogen and like the release of glucose 1-phosphate from glycogen, this process required GDE for continuous release.

Protein glycosylation defects in astrocytes and brains with aberrant glycogen storage

Given the substantial amount of glucosamine in brain glycogen, we hypothesized that knockdown of *PYGB* with a small hairpin RNA (shRNA) would reduce free glucosamine and alter the amounts of N-linked glycans. We performed *shPygb* knockdown in primary astrocytes (Figure 4A) and performed targeted analysis of free metabolites and protein glycosylation under glucose excess condition. Analysis of the *shPygb* astrocytes revealed that glycogen-derived glucose and glucosamine were increased in *shPygb* cells as predicted (Figure 4B). *Pygb* knockdown resulted in a mild but significant increase in intracellular free glucose 6-phosphate (Figure 4C), a key substrate for hexosamine pathway production of UDP-GlcNAc. Conversely, free glucosamine, free UDP-GlcNAc, and glycan-derived GlcNAc were all dramatically reduced (Figure 4C, 4D). To confirm that reduced UDP-GlcNAc alters the glycan profile in PYGB-deficient cells, we used wheat germ agglutinin (WGA), a lectin that binds GlcNAc, to probe the overall amount of glycosylated protein in

shPygb cell extracts. WGA conjugated to magnetic beads was used to enrich total glycosylated proteins, which were detected after separation by SDS-PAGE. Compared to the control cells infected with empty vector, *shPygb* cells displayed dramatically lower amounts of glycosylated protein (Figure 4D).

Since glucose 6-phosphate levels did not decrease, this result suggests that glucose from glycogenolysis is not a major contributor to the hexosamine pathway in *shPygb* cells cultured in excess glucose. To further assess the impact of *shPygb* on the hexosamine pathway, we performed stable-isotope tracing of UDP-GlcNAc using $^{13}C_6$-glucose as a substrate. At isotopic steady state, the fractional isotopologue pattern of UDP-GlcNAc represents metabolic precursors from glucose metabolism by glycolysis, pentose phosphate pathway, and the Krebs cycle (Figure 4E) (Moseley et al., 2011; Sun et al., 2017). We observed increased enrichment from $^{13}C_5$, $^{13}C_6$, $^{13}C_7$, and $^{13}C_8$ isotopologues of UDP-GlcNAc in *shPygb* cells compared to control (Figure 4F), indicative of increased glucose utilization for the synthesis of UDP-GlcNAc. Collectively, *shPygb* cells displayed a mild increase in intracellular glucose 6-phosphate and a marked increase in hexosamine pathway activity, yet the total pool of UDP-GlcNAc and protein glycosylation is compromised in *shPygb* cells. These results indicate that glucosamine released from glycogen servers as a critical physiological precursor metabolite for GlcNAc and N-linked glycan production (Figure 4G).

These results have direct implications for PGB-related diseases. We hypothesized that glucosamine sequestered in aberrant brain glycogen molecules as PGBs results in reduced glycan biosynthesis. Laforin, which is encoded by the gene *EPM2A*, is a glycogen phosphatase involved in glycogen metabolism (Nitschke et al., 2013; Tagliabracci et al., 2007; Worby et al., 2006). Deficiency in laforin function causes Lafora disease (LD), which is both a GSD and a cause of pediatric neurodegenerative epilepsy that typically results in death within ten years of disease onset (Gentry et al., 2018). Cytoplasmic PGBs form in cells from nearly all tissues in LD patients, including astrocytes and neurons throughout the brain (Augé et al., 2018; Ng and Turnbull, 2016; Rubio-Villena et al., 2018). Compared with glycogen in healthy tissue, the glycogen stored in LD PGBs is elevated, hyperphosphorylated, and exhibits perturbed branching (Irimia et al., 2015; Nitschke et al., 2013; Tagliabracci et al., 2007) (Figure S4A-E).

To test our hypothesis, we used laforin knockout (LKO) mice, a genetically engineered LD mouse model. Targeted mass spectrometry metabolomics of brains from wild-type or LKO mice indicated that glycan-derived GlcNAc, free glucosamine, and UDP-GlcNAc were dramatically decreased (Figure S4F). Similar to *shPygb* astrocytes, brains from LKO mice had increased amounts of glycogen-derived glucosamine (Figure S4F). Additionally, the brains from the LKO mice displayed markedly lower amounts of glycosylated proteins compared to the brains from wild-type mice (Figure S4G). Therefore, aberrant glycogen in the form of PGBs affects free glucosamine that consequently influences protein N-glycosylation.

Protein glycosylation defects in brain regions with PGBs in LKO mice

GlcNAc is the basic building block for the initiation of N-glycan biosynthesis (Stanley et al., 2017). Our results with the LKO mouse brains indicated that by sequestering glycogen, PGBs impaired protein N-glycosylation, which should be evident by a reduction in N-glycan abundance. We developed a novel workflow to evaluate the relationship between PGBs, glycogen, and N-glycan abundance in specific brain regions. We used matrix-assisted laser desorption/ionization (MALDI) coupled with traveling-wave ion-mobility high-resolution mass spectrometry (TW IMS) (Figure 5A). Formalin-fixed paraffin-embedded brain sections were treated with peptide-N-glycosidase F (PNGase F) and isoamylase applied by a high-velocity robotic sprayer (Powers et al., 2013). PNGase F releases protein-bound N-linked glycans, and isoamylase cleaves the glycogen α-1,6-glycosidic bonds to release linear oligosaccharide chains from 3 – 25 glucose units in length. TW IMS separates oligosaccharides and N-linked glycans based on differential collision cross section (Huang and Dodds, 2013) (Figure S5A). With this method, we quantitatively imaged glycogen, by combining linear chain polysaccharides between 4 – 15 sugar monomers, and specific N-glycans of various compositions within the brain sections (Figure 5B, C).

We compared the distribution of glycogen and N-glycans in brains of wild-type and LKO mice (Figure 5D, E; Figure S5B, S5C). As a validation of the method, we also performed immunohistochemistry with antibodies recognizing PGBs and glycogen (Figure 5E, S5D). In wild-type mice, glycogen was most abundant in the frontal cortex (Figures 5D, E). In contrast, the LKO mice had abundant PGBs in the cerebellum, hindbrain, midbrain, and the hippocampus (Figures 5D, E). This PGB distribution was similar to previous reports (Ganesh et al., 2002; Yokota et al., 1988). In addition to increased glycogen, the LD mouse brains exhibited decreases in three of the most abundant N-linked mouse brain glycans (Figures 5C, D and S5C). An overlay of glycogen and glycan MALDI images revealed dramatic reductions of N-linked glycans in areas of PGB (glycogen) accumulation (Figure 5E). We expanded the glycan profiling using a Fourier-transform mass spectrometer (FTMS) with sufficient sensitivity to detect larger N-glycan structures (Powers et al., 2013). Throughout the LD mouse brain, we observed decreased N-linked glycans of most structures (Figure S5E-F).

To assess if altered glycosylation correlated with cellular responses, we performed immunohistochemical analyses to evaluate XPB1 and GRP78, markers of the unfolded protein response (UPR) and ER stress. We focused on the hippocampus, brainstem, and thalamus, because these were regions with high PGB levels (Figure 5D). Adjacent sagittal whole brains slices were stained for XBP1 and GRP78 (Figure S5G), and we detected increases in both markers, consistent with previous findings (López-González et al., 2017). Neuroinflammation is associated with ER stress (Deslauriers et al., 2011). We also detected increased staining for the neuroinflammation markers IBA1 and GFAP (Figure S5G). Thus, our data indicated that regions with high amounts of PGBs lack available glucosamine to glycosylate proteins appropriately, which initiates an ER stress response and neuroinflammation.

Glycosylation defects in a GSD III mouse model

GDE is a key enzyme during glycogenolysis and possesses two independent catalytic activities: oligo-1,4→1,4-glucanotransferase activity transfers 3-glucosyl molecules to the neighboring chain for release by GP, and amylo-1,6-glucosidase activity removes the terminal glucosyl molecule, releasing glucose (Adeva-Andany et al., 2016). Loss-of-function mutations in GDE results in GSD type III (Figure 6A). Aberrant glycosylation in apolipoprotein C-III has been previously reported in this disease (Ondruskova et al., 2018). We hypothesize that *Gde* knockout mice would result in glycogen sequestration of glucosamine and altered N-linked glycosylation. We utilized a whole body *Gde* KO mouse (Figures 6B, C), which is predicted to be a genetic model of human GSD type III (Kishnani et al., 2010). Similar to the human disease, the *Gde* KO mice had increased glycogen deposits in skeletal muscle and liver (Figure 6D). Consistent with the human disease, the glycogen isolated from *Gde* KO mice has significantly higher numbers of short glucose chains compared to glycogen isolated from wild-type mice (Figure 6D). *Gde* KO mice also exhibited GSD III clinical features, such as hypoglycemia, reduced circulating lactic acid, and increased activities of the liver enzymes of alkaline phosphatase, alanine aminotransferase, and aspartate aminotransferase (Figure S6A, S6B).

Similar to *shPygb* cells and LKO mice, brains from *Gde* KO mice had higher amounts of glycogen-derived glucose, increased glycogen-derived glucosamine, and decreased glycan-derived GlcNAc (Figure 6E). Collectively, these results indicate that the brains of the *Gde* KO mice exhibited glycogen accumulation and impaired protein N-glycosylation. Targeted metabolomics analyses of polar extracts from brains of wild-type and *Gde* KO also revealed significant decreases in the available pool of free glucose, glucosamine, and UDP-GlcNAc (Figure 6E). Thus, this additional GSD mouse model supports the hypothesis that glycogen metabolism is directly connected to glycosylation by modulating the free intracellular glucosamine pool (Figure 6F). Furthermore, our data with both mouse models demonstrates that aberrant glycan metabolism is a brain-centric feature of these two GSDs and results in impaired protein glycosylation.

Enzymatic hydrolysis of PGBs rescues hypoglycosylation

Thus far, we have demonstrated that glycogen-derived glucosamine is a critical substrate for protein glycosylation and that aberrant PGBs in GSD mouse models result in protein hypoglycosylation. We previously developed the antibody-enzyme fusion VAL-0417 comprised of a cell-penetrating antibody fragment and pancreatic α-amylase (Austin et al., 2019; Brewer et al., 2019). We found that continuous intracerebroventricular (i.c.v.) administration of VAL-0417 for 7 days into the cerebral lateral ventricle of 7-month old LKO mice ablated LD PGBs throughout the brain and rescued the brain metabolic defect in LKO mice (Brewer et al., 2019). We hypothesized that enzymatic hydrolysis of aberrant PGBs by VAL-0417 would also rescue the LKO protein hypoglycosylation defect. To test this hypothesis, we performed MALDI glycogen and glycan imaging on LKO brains that had been i.c.v. treated with PBS or VAL-0417 as well as WT. As previously reported by microscopy, VAL-0417 cleared LKO brain PGBs in the cerebellum, midbrain and brain stem (Figure 7A). In the same brain slice, we also observed rescue of major classes of N-linked glycans, including high mannose, hybrid, and complex N-glycans when compared to the

same glycans in LKO brains treated with PBS and WT brains (Figure 7A-B, S7A-B). These data suggest the N-linked glycan pathways are still functional in the LKO brain and that substrates released from PGB hydrolysis can be utilized for *de novo* N-linked glycan production (Figure 7C).

Discussion

This study defines a critical novel and direct link between glycogen metabolism and N-linked protein glycosylation. Our results indicate that brain glycogen is a critical glucosamine reservoir. Furthermore, we demonstrated that glucosamine incorporation and release from glycogen occurs through the canonical glycogen metabolic enzymes GYS and GP. Structural analysis revealed a mechanism of glucosamine transfer from UDP-glucosamine to glycogen by GYS analogous to the transfer of glucose. Both the 2'-NH_2 and 2'-OH groups of glucosamine are capable of acting as hydrogen bond donors within the growing glycogen sugar chain.

Dysregulated glycogen metabolism directly altered intracellular pools of glucosamine, UDP-GlcNAc, and the level of protein N-glycosylation. The physiological importance of these findings was demonstrated with primary astrocyte cultures and two GSD mouse models. This study highlights the power of studying rare genetic diseases to expand fundamental knowledge of cell biology and biochemistry, while simultaneously elucidating disease pathology. Indeed, we defined that glucosamine composition varies dramatically between brain, liver, and muscle glycogen. The brain contains less glycogen-derived glucose than the liver and muscle, but it contains a significantly higher percentage of glycogen-derived glucosamine when normalized to tissue mass.

Our data establish that dysregulated glycogen metabolism, resulting in PGBs, leads to defects in protein glycosylation. Abnormal glycosylation has been reported clinically in GSD type Ib, III, IV, and XIV (Den Hollander et al., 2007; Ondruskova et al., 2018). Additionally, profound protein hypoglycosylation was observed in patients with mutation in the ER-associated glucose 6-phosphate transporter that results in GSD Ib (Hayee et al., 2011). This defect is even more apparent in patients with congenital deficiency of phosphoglucomutase (PGM1), the enzyme that transfers glucose phosphate from the 1’ to 6’ position. Loss of PGM1 activity results in both PGB accumulation and protein hypoglycosylation, resulting in the disease being classified as GSD XIV and a CDG (Adeva-Andany et al., 2016). Moreover, loss-of-function mutations in phosphomannomutase 2 that generates mannose 6-phosphate also yields aberrant glycogen aggregates that often leads to misdiagnosis as a GSD based on histopathology analysis (Choi et al., 2015). These clinical data support the finding that glycogen and N-linked glycosylation are intimately connected. This study provides mechanistic insights at the molecular level elucidating a metabolic connection between glycogen and glycosylation.

We found that ~25% of brain glycogen is glucosamine, which represents a substantial pool of glucosamine for protein glycosylation. Our data suggest that the brain prefers *de novo* synthesized glucosamine rather than exogenous sources. This result is not surprising as the blood brain barrier limits nutrient availability other than glucose for the brain; and *de novo*

synthesis would offer additional intra-cellular regulatory steps that could be useful during adverse conditions. The unique composition of brain glycogen suggests an alternative, tissue-specific role that has been previously overlooked. Regulation of glycogen metabolism through posttranslational modifications is well-characterized and occurs immediately upon stimuli (Roach et al., 2012). Thus, astrocytes and neurons have adapted to modulate the glucosamine pool availability in response to different extracellular stimuli and physiological conditions. In GSDs impacting the brain, in which efficient glycogenolysis does not occur, cells adapt by altering their transcriptional and metabolic landscapes, especially the hexosamine pathway in response to the lack of available glycogen-derived glucosamine. In LD, our results suggest that this glucosamine deficiency results in UPR and ER stress. We propose that chronic exposure to UPR and ER stress are key drivers for GSDs in the brain, including LD.

Intriguingly, glycogen molecules are frequently observed adjacent to the ER membrane by electron microscopy (Garant, 1968; Mandl and Bánhegyi, 2018). This physical proximity could enable a mechanism for compartmentalized glycogenolysis coupled with the initiation of N-linked glycan biosynthesis. Our previous work demonstrated that nuclear glycogen supplies a substrate for histone acetylation (Sun et al., 2019). Thus, glycogen is more than just an energy cache. In addition to serving as a source of molecules for histone acetylation, glycogen is also an integral part of the N-linked glycan biosynthetic pathway. Our data suggest that glucosamine is the primary substrate for N-linked glycan biosynthesis during glycogenolysis. This result is not entirely surprising as glucose released from glycogen is critical in maintaining brain bioenergetics, for example the glycogen-pyruvate-lactate shuttle has been proposed in astro-glia-neuronal metabolism (Pellerin, 2003). However, this does not exclude glycogen-derived glucose from participating in hexosamine metabolism. The metabolic interplay between glycogenolysis and N-linked glycan metabolism should be rigorously assessed in neurological disorders where glucose availability is reduced such as dementia or traumatic injuries in future studies.

This study reveals that glucosamine is utilized in three distinct pools: as a free metabolite, glycogen-bound, or utilized to produce GlcNAc in branched glycans and poly-mannose chains, and demonstrates that the interplay between these three glucosamine compartments is crucial to maintaining homeostatic brain metabolism. Direct hydrolysis of PGBs in LKO mice using an enzyme therapeutic approach resulted in the rescue of protein N-linked glycosylation. With the aid of the new MALDI imaging workflow for glycogen and glycans, we discovered the negative correlation between glycogen and N-glycans in WT and LKO mice. These insights are not possible with traditional analyses that involve whole brain homogenates (Brewer et al., 2019). To this end, the MALDI imaging workflow could prove to be a valuable tool in assessing response to therapy in the future preclinical/clinical development of therapeutics targeting GSDs or CDGs. Finally, glucosamine flux through glycogen could be a critical component of aging and under stress stimuli, such as traumatic brain injury and dementia, since aberrant glycosylation has been reported for these diseases (Endo, 2005; Kizuka et al., 2017).

Limitation of the study.

In this study, we identified a previously unknown route of N-linked glycan biosynthesis through glycogen metabolism, yet several interesting questions remain to be answered. 1) We identified that astrocytes prefer to utilize *de novo* synthesized glucosamine for incorporation into glycogen. The enzymes responsible for these actions and their regulation remain to be characterized for the metabolic conversation of glucose to glucosamine and UDP-glucosamine. 2) This study focuses on N-linked glycans but UDP-GlcNAc is also utilized for protein O-linked glycosylation, protein O-GlcNAcylation, biosynthesis of proteoglycans and gangliosides of the brain (Andres et al., 2020a). Therefore, glucosamine phosphate release from glycogenolysis is likely important for these pathways as well. Development of imaging technologies for simultaneously profiling polar metabolite intermediates and additional classes of protein linked GlcNAc would aid in expanding our understanding of complex carbohydrate metabolism of the brain.

STAR Methods

Resource availability

Lead Contact: Further information and requests for resources and reagents should be directed to and will be fulfilled by the Lead Contact, Matthew Gentry (matthew.gentry@uky.edu).

Material availability: This study did not generate new and unique plasmids or mouse models. Recombinant proteins and synthesized nucleotide sugars are available from the corresponding authors on reasonable request.

Data and code availability: Structure of UDP-glucosamine bound yGys2 is deposited in the protein data bank (PDB): identifier 5UW4. The published article includes all other datasets generated and analyzed during this study.

EXPERIMENTAL MODEL AND SUBJECT DETAILS

Generation of primary astrocytes cell lines—Generation and maintenance of primary astrocytes cultures was based on the procedure previously described (Walls et al., 2014). Seven-day-old C57/BL6 mice were euthanized by decapitation followed by dissection and isolation of the frontal cortex. The cortex tissue of all mice (males and females mixed) was carefully processed through an 80 μM sieve into 10 ml of Dulbecco's Modified Eagle Medium (DMEM) + 20 % fetal bovine serum (FBS). The cells were further mechanically separated by trituration before the cell suspension was diluted and seeded in 25-cm^2 flasks and stored in a CO_2 incubator (5% CO_2, 21% O_2) at 37°C. Media was changed after two days and subsequently replenished on a 2-day interval. The cells were cultured for three weeks with decreasing FBS concentration: 1st week 20% FBS, 2nd week 15% FBS, and 3rd week 10% FBS. Dibutyryl cyclic AMP (dBcAMP) was added to the media in the last week of culturing to mature the astrocytes and promote glutamate transporter expression. For the generation of glycogen phosphorylase (GP) brain isoform knock down primary astrocytes (shPygb), lentivirus carrying either empty vector (EV) or shPygb (Santa Cruz

Biotechnology) were added to the astrocytes in serum-free media at the multiplicity of infection (MOI) of 3:1 for 24 hours followed by the replacement of normal culture media. Knockdown efficiency was confirmed at 72 hours by immunoblotting for Pygb.

Mouse models—Mice were housed in a climate-controlled environment with a 14 (light)/10 (dark) hours cycle (lights on at 0600 hours) with temperature and humidity maintained at 72°F (22°C) and at least 30%, respectively, and water and solid diet (LabDiet 2018, St. Louis, MO, except during tracer administration which received liquid diet, see below) provided *ad libitum* throughout the study. All animals were housed in shoebox caging with filter tops measuring at 18.5 cm W x 30 cm D x 12 cm H (Alternative Design, Siloam Springs, AR) on corncob bedding (Bed O' Cob, Andersons, Maumee, OH) under static conditions. All mice were provided with tissue material for nesting. Both males and females were housed in the same room. Indirect sentinels were utilized to assess colony health that include general alertness, coat color, hair loss, weight loss, physical trauma, and gross movement. At the time of these studies, the colony was free of mouse parvovirus, mouse coronavirus, mouse theliovirus, pneumonia virus of mice, Sendai virus, Reovirus 3, mouse rotavirus, lymphocytic choriomeningitis virus, Mycoplasma pulmois, and ectoparasite and endoparasites. The institutional animal care and use committee at University of Kentucky has approved all of the animal procedures carried out in this study under PHS Assurance #A3336-01. *Epm2a*$^{-/-}$ mice, referred to as laforin knockout (LKO), were previously described (Ganesh 2002 HMG). In brief, DNA sequence encoding the laforin dual specificity phosphatase domain was replaced with a neomycin domain. For the generation of glycogen debranching knockout mice (GdeKO), a heterozygous C57BL/6N-AGLTm1aWtsi/H mouse was purchased from the MRC Harwell Institute which distributes mice on behalf of the European Mouse Mutant Archive (www.infrafronIer.eu; Repository#EM:05784). This mouse line originated from an ES cell clone (clone id EPD0371_2_E12) in which a knockout targeting cassette - mouse engrailed 2 gene splice acceptor (En2 SA) and poly(A), the beta-galactosidase (lacZ gene), the neomycin-resistance (neo gene), FRT, and loxP sites - was inserted between exons 5 and 6 of the *Gde* gene. This construct results in the loss of the exons downstream of exon 5 that contain the C-terminal 1310 amino acids encoding the glucosyl transferase and glucosidase catalytic domains. Breeding and intercrossing of the heterozygous mice generated wild-type (WT), heterozygous, and homozygous animals. The genotype was confirmed by PCR analyses using primers recommended by the Harwell Institute that produce 230 and 106 bp fragments for the WT and mutant allele, respectively. The antibody used to detect Gde by Western blotting (Abcepta, AP2402c) was raised to a region between amino acids 15 and 35. Because the 25 kDa N-terminal polypeptide could not be detected, this indicates that either the N-terminal 220 amino acid protein fragment is unstable, or the mRNA undergoes nonsense-mediated decay. All studies used ~5-month-old mice, were conducted in accordance with federal guidelines, and were approved by the Institutional Animal Use and of Indiana University or University of Kentucky. Blood glucose and lactate were measured in fed and overnight fasted mice from tail snips using a Bayer Contour Blood Glucose Meter and an Arkray Lactate Pro Blood Lactate Meter, respectively. Liver enzymes were measure in serum, collected at the time of euthanasia using a Fuji Dri-ChemClinical Chemistry Analyzer FDC 3500. Periodic acid-Schiff (PAS) staining of skeletal muscle of WT and Gde

knockout mice (male and female) was performed by the Histology Core in the Department of Anatomy and Cell Biology, Indiana University School of Medicine previously described (DePaoli-Roach et al., 2010). Briefly, sections were prepared from 3-month old mouse tissues fixed in 10% formalin and embedded in paraffin. 5μm sections were deparaffinized, and oxidized with 0.5% periodic acid for 5 min, stained with Schiff reagent for 15 min, and counterstained in hematoxylin and eosin for 15 min.

METHOD DETAILS

Western blotting—Whole-cell extracts were generated in RIPA buffer (0.5% deoxycholate, 1% IGEPAL-CA630, 0.1% sodium dodecyl sulfate, 150 mM NaCl, 50 mM Tris-8.1), lysates were cleared by centrifugation, and protein concentrations were quantified via the Pierce BCA Protein Assay Kit (Thermo). For protein SDS-PAGE separation, 25 μg of protein extract per sample was denatured with heat and reducing agents, separated on a 4–12% acrylamide gel (BioRad) and transferred to PVDF (BioRad). Antibodies for Western blotting recognized Pygb (LSBio, 1:1,000) and rhodamine-conjugated anti-tubulin antibody (Bio-Rad, 1:5000). All antibodies have detailed species validation available online from vendors. The StarBright Blue 700 fluorescent secondary anti-rabbit IgG antibody (BioRad, 1:5,000) was incubated for 1 hour at room temperature. After washing, fluorescent images were acquired using a ChemiDoc MP (BioRad). Western blots were performed a minimum of three independent experiments and the results are representative of a single experiment.

Wheat germ agglutinin (WGA) blotting—Whole-cell extracts were generated in RIPA buffer (0.5% deoxycholate, 1% IGEPAL-CA630, 0.1% SDD, 150 mM NaCl, 50 mM Tris-8.1), lysates were cleared by centrifugation, and protein concentrations were quantified with the Pierce BCA Protein Assay Kit (Thermo). For protein SDS-PAGE separation, 25 μg of protein extract per sample was denatured with heat and reducing agents, separated on a 4–15% TGX Stain-Free Precast acrylamide gel (BioRad) and transferred to PVDF (BioRad). Total protein was imaged by the ChemiDocMP immediately from both gel and PVDF membrane using manufacturers settings. PVDF membrane is incubated in PBS containing 2% TWEEN 20 for 2 min at 20°C, rinsed two more times with PBS before incubation with 5 μg of peroxidase conjugated WGA (Sigma) in 5 ml of PBS with 1 mM $CaCl_2$, 1 mM $MnCl_2$, and 1 mM $MgCl_2$ for 16 hours at room temperature. At the end of the incubation, membrane is washed twice with PBS, and images were acquired using the ChemiDocMP (BioRad) using the Clarity Max ECL HRP Substrate.

Immunohistochemistry—Mice were sacrificed by cervical dislocation followed by immediate brain extraction and fixation in neutral-buffered 10% formalin (NBF) then paraffin embedded and stored prior to use. Fixed mouse brains were sectioned at 10 μm and immunohistochemistry was performed at the University of Kentucky Biospecimen Procurement and Translation Pathology Shared Resource Facility using the method previously described (Zhang et al., 2017). Briefly, slides were dewaxed, rehydrated and warmed to 37°C for 1h in Ventana CC2 standard buffer for antigen retrieval. Following antigen retrieval, tissue sections were incubated in primary antibodies for 60min at room temperature followed by secondary antibody for 60min at room temperature. Antibodies used for immunohistochemistry recognized Grp78 (LSBio), Gfap (Abcam), Xbp1 (Abcam),

Iba1 (Abcam), and glycogen [IV58B6, gift from Dr. Baba (Baba, 1993)]. Digital images were acquired through the ZEISS Axio Scan.Z1 high resolution slide scanner. Image analysis was performed using the HALO software (Indica labs).

Cell culture, ^{13}C enrichment, and washout labeling in cultured astrocytes—For the tracer experiment, 21-day matured primary astrocytes were incubated in base growth media supplemented with either 10 mM $^{13}C_6$-glucose or 2 mM $^{13}C_6$-glucosamine, in a CO_2 incubator maintained at 37°C. At the end of 30 min, 1, 2, 4, or 8 hr incubation periods, cells were washed with cold PBS three times followed by extraction with methanol/water/chloroform (V/V 2:1.5:1) and separated into polar, lipid, and insoluble fractions. The insoluble fraction was further processed to separate glycogen from proteins and their bound N-glycans. For washout experiments, primary astrocytes were first incubated with ^{13}C-glucose for 8 hr, then base growth media with $^{12}C_6$-glucose were added back to the cultures in the presence and absence of 1,4-dideoxy-1,4-imino-d-arabinitol (DAB) followed by the isolation of glycogen at 30 min, 1, 2, 4, or 8 hr from separate cell cultures. Monomeric carbohydrates and amino sugars and their labeling patterns were released by acid hydrolysis, which were detected by GCMS analysis.

***In vivo* ^{13}C-glucose labeling of mice—**A liquid diet base containing casein, L-cystine, soy oil, cellulose, mineral mix (AIN-93G-MX), calcium phosphate, vitamin mix (AIN-93-VX), choline bitartrate, tert-butylhydroquinine (TBHQ), and xanthan gum was purchased from Harlan Laboratories (Madison, WI). $^{13}C_6$-glucose was obtained from Cambridge Isotope Laboratories (Tewkebury, MA). For the tracer study, unlabeled glucose and water were added to the base diet two days prior to the tracer study to give a final diet of 0.167 g glucose/g diet and a net protein content of 53 mg/g diet to provide sufficient carbon and nitrogen according to the vendor. Mice (20 g body weight) were fed 13.6 g liquid diet (at 680 g diet/kg mouse). This pre-feeding of unlabeled liquid diet served to accustom the mice to the liquid diet feeding. On the third day, $^{13}C_6$-glucose at 0.173 g/g diet replaced the unlabeled glucose in the diet for each mouse and the mice were allowed to consume the diet ad libitum for 18 h. At the end of the feeding period, mice were sacrificed by cervical dislocation, and brains were harvested and snap frozen in liquid nitrogen.

Metabolite analysis by NMR spectroscopy—NMR spectra were recorded at 14.1 T and 15°C on a Varian DD2 spectrometer equipped with a 3 mm inverse triple resonance cold probe. 1D ^1H NMR spectra were recorded with an acquisition time of 2 s, a recycle time of 6 s to minimize peak saturation, and continuous rf presaturation of the residual water resonance at 4.88 ppm. 1D ^1H-{^{13}C} HSQC spectra were recorded with an acquisition time of 0.25 s, a recycle time of 2 s, and adiabatic decoupling of the ^{13}C. Proton spectra were typically processed with zero filling to 131k points, and apodized with an unshifted Gaussian and a 0.5 Hz line broadening exponential. HSQC spectra were processed with zero-filling to 16 k points and apodized using an unshifted Gaussian function and 4 Hz line broadening. Concentrations of metabolites and ^{13}C abundance were determined by peak integration of the ^1H or HSQC NMR spectra referenced to the intensity of DSS-d6 methyl protons, with correction for differential relaxation.

Enzymatic synthesis of uridine-5′-diphospho-2-deoxy-2-fluoro-α-D-glucopyranose (UDP-2FGlc) and uridine-5′-diphospho-D-glucosamine (UDP-glucosamine)—The synthesis of UDP-2FGlc was adapted from (Olaf Prante, 2007) and the synthesis of UDP-glucosamine was adapted from (Ma and Stockigt, 2001). The enzymatic synthesis of UDP-2FGlc used FDG as the starting material and the synthesis of UDP-glucosamine was initiated from D-glucosamine-6-phosphate. The following commercial enzymes were utilized: hexokinase, phosphoglucomutase (PGM), inorganic pyrophosphatase, alkaline phosphatase and pyruvate kinase. *Leishmania major* UDP-sugar pyrophosphoryrlase (LMUGP) was prepared as previously described (Lamerz et al., 2006). Briefly, the open reading frame with primer pair ACM112 and ACM69 was amplified with Ndel and Notl restriction sites. The resulting PCR product was ligated into the corresponding sites of pET22b (Novagen). The resulting plasmid pET-UGP-His encodes the full-length, C-terminally His6-tagged L. major UGP. For expression, *E. coli* BL21(DE3) were transformed with the corresponding plasmid, and cells were grown in Luria-Bertani medium with 200 μg/ml carbenicillin at 15 °C to an A_{600} nm of 0.6. Bacteria were lysed by sonification with a microtip and cell debris was removed by centrifugation. The soluble fractions were used for SDS-PAGE analyses or submitted to Ni2+-chelating or anion exchange chromatography to purify the recombinant protein. All enzymes were prepared for use in 20 mM Tris·HCl, pH 7.8.

Synthesis of UDP-2FGlc was performed in two steps. The first step was performed at 30°C using a 4-hour incubation. The final reaction volume was 10 mL and contained 100 mM Tris·HCl, pH 7.8, 25 mM UTP, 22.2 mM FDG, 37.5 mM $MgCl_2$, and 250 Units hexokinase. The reaction was monitored by high-performance anion exchange chromatography (HPAEC) analysis. Upon completion, the enzyme was denatured by heating at 100°C for 5 min. After centrifugation to remove the denatured enzyme, 5 mL of the hexokinase reaction supernatant was added to 45 mL of a solution containing 50 mM Tris·HCl, pH 7.8, 5 mM $MgCl_2$, 44 μM G1,6PP, 5 mM PEP, 500 Units pyruvate kinase, 200 Units PGM, 20 mg of LMUGP, and 200 Units of yeast inorganic pyrophosphorylase. After mixing, the reaction mixture was filtered with a 0.22 μm membrane and incubated overnight at 30°C. The enzymes were denatured by heating at 100°C for 2 min, and the denatured enzymes were removed by centrifugation. Finally, 200 Units of alkaline phosphatase was added to hydrolyze any residual nucleotide phosphates.

Synthesis of UDP-glucosamine was carried out in a single reaction, which was incubated overnight at 30°C. The reaction was monitored by high-performance anion exchange chromatography (HPAEC) analysis. The reaction mixture consisted of 50 mM Tris–HCl, pH 7.8, 5 mM $MgCl_2$, 2 mM $GlcNH_2$-6-phosphate, 4 mM phosphoenopyruvate (PEP), 2 mM UTP, 40 μM glucose-1,6-diphosphate, 1000 Units PGM, 10 mg of LMUGP, 200 Units of yeast inorganic pyrophosphorylase, and 500 Units of pyruvate kinase in a total reaction volume of 200 ml.

Purification of UDP-2FGlc and UDP-glucosamine—Purification involved two chromatographic steps, activated charcoal and batch DEAE-cellulose anion exchange chromatography. The reaction mixtures were added to 5 g of activated charcoal and incubated for 10 min, before pouring the mixture into a sintered glass funnel and removing

the liquid by vacuum filtration. The charcoal was washed three times with 100 mL of ice-cold water. The UV absorbance of the wash solution was monitored at 262 nm to ensure no loss of UDP-2FGlc from the charcoal. The bound UDP-sugars were eluted using 50% ethanol containing 0.16 M NH_4OH. The pH of the samples was adjusted to pH 7 using acetic acid before evaporation using a rotary evaporator operated at 40°C under reduced pressure (Dhugga and Ray, 1994). DEAE-cellulose (100 g) was equilibrated with 1 L of 10 mM ammonium acetate, pH 5.0.

For anion exchange chromatography, the sample was adjusted to pH 5.0 and then the sample was bound to the resin using a batch method by incubating resin and sample for 1 hour at room temperature. The resin/sample mixture was transferred to a sintered glass funnel and the liquid was removed by vacuum filtration. The resin was washed with 10 mM ammonium acetate, pH 5.0 until the UV absorbance at 262 nm was below 0.1 for the wash fractions. Bound UDP-sugars were eluted with 100 mM ammonium acetate, pH 5.0. The eluted fractions were adjusted to pH 6 and the volume reduced through evaporation using a rotary evaporator and then reduced to dryness by lyophilization. Excess acetic acid was removed by repeated lyophilization. The purification process was monitored by HPAEC analysis.

Both UDP-2FGlc and UDP-glucosamine were obtained at a chemical purity of >95% as judged by HPAEC analysis. LC/MS analysis verified the identities of the compounds. The purified UDP-2FGlc and UDP- glucosamine (25 μL of a 100 μM solution) were injected into an Agilent 6520 quadrupole time-of-flight mass spectrometer operating in both positive and negative ion electrospray mode. The data were analyzed using the Mass Hunter software. The purity of the synthesized UDP-sugar donors was > 95 % by LC/MS.

HPAEC analysis of the sugar nucleotides—The ability of yGsy2 to catalyze the hydrolysis of UDP-sugars was determined by incubating 5 μM of yGsy2 with a solution containing 1 mM glucose 6-phosphate (G6P) and 100 μM of the different UDP-sugars in a final volume of 100 μL. The reactions were performed in a final volume of 50 μL, the first of which was designated t_0 and immediately terminated while another reaction ($t_{O/N}$) was incubated at room temperature for 16 hours. Both were terminated by boiling. All samples were filtered prior to analysis on the HPAEC using a Dionex ICS3000 system and its associated Chromeleon software; the analytical method used was adapted from Tomiya *et. al.* (Tomiya et al., 2001). The separation of analytes was accomplished using a 2 x 250-mm CarboPac PA1 column (Dionex) operated at a flow rate of 0.25 ml/min using 1 mM sodium hydroxide (NaOH, eluent A), and 1 mM NaOH containing 1 M sodium acetate (NaOAc), eluent B. The analysis method included 3 gradient steps: (i) 20 – 50% eluent B, 0 – 10 min, (ii) 55 −8 5% eluant B, 10 – 35 min and (iii) 85 −100% eluant B, 35 – 40 min. As standards, 100 μM UDP and 10 μM of UMP were passed through the HPAEC column. Hydrolysis of UDP-glucose analogs was evaluated by the decrease in the peak volume of the UDP-glucose analogs and the appearance of new peaks corresponding either to UMP or UDP.

Expression and purification of recombinant enzymes—His-tagged yGsy2 recombinant enzyme was expressed in BL21 (DE3) *Escherichia coli* (New England BioLabs) and purified as described previously using affinity and ion-exchange chromatography (Baskaran et al., 2010). The purified enzyme was stored in 20 mM Tris-

HCl, pH 8.0 and 1 mM 2-β-mercaptoethanol (BME) buffer at −80°C until use. Human glycogen debranching enzyme (GDE) and glycogen phosphorylase (PYGB) was expressed in BL21(DE3) strain from the pPB-His-GST-AGL protein expression plasmid (ABG Good, cat. no. 115220220300) in 2×YT medium: 16 g/L tryptone, 10 g/L yeast extract, 5 g/L NaCl; supplemented with 50 mg/L kanamycin, and 17 mg/L chloramphenicol. Induction was achieved with 400 μM isopropyl-β-D-thiogalactopyranoside for 16 hours at 16°C upon reaching an OD_{600} of 0.5. Bacteria were harvested by centrifugation (5,000*g*, 15 min, 4°C) and resuspended in homogenization buffer (50 mM HEPES, pH 7.4, 50 mM KCl, 100 mM NaCl, 2 mM dithiothreitol) supplemented with one tablet of protease inhibitor cocktail (Roche Applied Science) per 50 mL buffer. Homogenization was achieved by incubation with 1 g/L lysozyme (Sigma) for 15 min at 4°C with gentle inversion followed by sonication. The homogenizations were cleared by centrifugation (25,000 *g*, 30 min, 4°C) and the cleared lysate incubated with glutathione-agarose resin (Gold Biotechnology) for 15 min at 4°C with gentle inversion. The agarose was then pelleted by centrifugation (3,000 *g*, 10 min, 4°C), washed with homogenization buffer thrice, and the bound recombinant protein eluted with 10 mM reduced glutathione in homogenization buffer and concentrated using an Amicon Ultra-15 50 kDa MWCO (Millipore).

yGys2 glucose and glucosamine elongation assay—Assays were performed in 50 μL and contained 50 mM HEPES, pH 7.4, 500 μg maltoheptaose (CarboExpert) and 1 mM UDP-glucose (Cayman Chemical) or UDP-glucosamine. Elongation was initiated by addition of 10 μg of purified yGys2 and incubate in a 30°C water bath for indicated number of hours. The reaction is quenched by adding an equal volume of methanol. A 5 μl aliquot of the reaction was spotted on a glass microscope slide, then dried in a desiccator prior to matrix application. α-cyano-4-hydroxycinnamic acid matrix (0.021 g CHCA in 3 ml 50% acetonitrile/50% water and 12 μL TFA) was applied using the HTX sprayer. For the detection of DP7, DP7+glucose, DP7+glucosamine, a Waters SynaptG2-Si high-definition mass spectrometer was used. The laser was operating at 1000Hz with an energy of 200AU and spot size of 100μm, mass range is set at 500-2000m/z. Results were processed and analyzed by using the Masslynx software (Waters).

yGys2 inhibition by UDP-sugar donors—The activity of yGsy2 was determined in the presence of competing concentrations of nucleotide sugar donors (UDP-2FGlc, UDP-galactose, UDP-glucosamine, or UDP-xylose) in the range 0.01 mM – 20 mM. For these assays, the concentration of UDP-Glc was 0.5 mM and the reactions with G6P contained 7.2 mM G-6-P. All kinetic data analyses were performed using the program package SigmaPlot (version 12.3) by fitting the data to the appropriate binding or kinetic equation. The IC_{50} curves for different UDP-sugar donors were fit to the four-parameter logistic equation. The values presented in this work are the averages ± the standard errors of the mean of three independent experiments with triplicate measurements for each data point in each experiment.

Crystallization and structure determination—The crystal complex of G6P bound yGsy2 enzyme and UDP-glucosamine were obtained using the hanging drop vapor diffusion method as described previously (Baskaran et al., 2010). Briefly, the protein solution was

prepared at 2.5 mg/ml containing 25 mM G-6-P and 10 mM of UDP-glucosamine. The protein solution was mixed with the crystallization reservoir solution containing 0.1 M Bis-Tris, pH 6.2-6.5 and 22-25% PEG300. The crystals were cryo-protected through coating with immersion oil and frozen in liquid nitrogen as previously described (Baskaran et al., 2010). The data sets were collected at the Advanced Photon Source at beamline 23-ID, operated by the GM/CA Collaborative Access Team. The data set was indexed, integrated and scaled by the XDS program package (Kabsch, 2010). The structures were solved by molecular replacement using the program MOLREP (Winn et al., 2011), as implemented in the Collaborative Computational Project Number 4 (CCP4) program (Collaborative Computational Project, 1994) suite. The search model for molecular replacement was the G6P-bound yGsy2 structure (pdb code: 3NB0). The refinement procedure utilized an initial single round of rigid body refinement for individual domains followed by iterative rounds of restrained refinement with the application of domain-based TLS and NCS restraints using REFMAC5 (Murshudov et al., 2011) as implemented in CCP4. COOT (version 0.7.2.1) (Emsley and Cowtan, 2004) was used to visually inspect and manually adjust the refined models. The interactions between the sugar nucleotides and surrounding amino acid residues were evaluated using the program Ligplot (Wallace et al., 1995).

Mouse tissue preparation for mass spectrometry analysis—Mice were sacrificed by cervical dislocation, brains were removed immediately post-mortem, and washed once with PBS, twice with diH_2O, blotted dry, and snap frozen in liquid nitrogen. For the Gde KO mice, equal numbers of male and female mice were used between the knockout and wildtype groups. The frozen tissues were pulverized to 5 μm particles in liquid nitrogen using a Freezer/Mill Cryogenic Grinder (SPEX SamplePrep). Pulverized tissue (20 mg) was extracted in 50% methanol/chloroform (V/V 1:1) and separated into polar (aqueous layer), lipid (chloroform layer), and protein/glycogen (interfacial layer) fractions. The polar fraction containing free metabolites was dried at 10^{-3} mBar using a SpeedVac (Thermo) followed by derivatization. Glycogen was separated from the protein pellet using 1.5 mL of ice cold 10% trichloroacetic acid. Complete removal of glycogen was confirmed by treating the protein fraction with amylase and the absence of released glucose signal. Isolated glycogen was dried by vacuum centrifuge at 10^{-3} mBar, resuspended in ddH_2O, and further purified by density displacement in a 4 – 20% sucrose gradient. Finally, any non-covalently bound small molecules were removed by dialysis against ultra-pure H_2O through a low-binding membrane with a 3.5 kDa cut off (Slide-A-Lyzer, ThermoFisher) for 18 hr at 4°C.

Hydrolysis of glycogen to monomeric sugars—Hydrolysis of glycogen was performed by first resuspending the pellet in diH_2O followed by the addition equal parts 4N HCl. Samples incubated at 95°C for 2 hr on a vortex mixer with a heated lid. The reaction was quenched with 100% methanol with 40 μM L-norvaline (as an internal control). The sample was then incubated on ice for at least 30 min. The supernatant was collected by centrifugation at 15,000 rpm at 4°C for 10 min and subsequently dried by vacuum centrifuge at 10^{-3} mBar.

Protein and N-glycan hydrolysis—Hydrolysis of the protein and bound N-glycans fractions were first dried by vacuum centrifuge at 10^{-3} mBar for 30 min. The pellet was

dissolved in diH_2O followed by the addition of equal part 2N HCl. Samples were incubated at 95°C for 2 hr on a vortex mixer with a heated lid. All reactions were quenched with 100% methanol with 40 μM L-norvaline. Samples were incubated on ice for 30 min, and the supernatant collected after centrifugation at 15,000 rpm at 4°C for 10 min. The collected supernatant was subsequently dried by vacuum centrifuge at 10^{-3} mBar.

Enzymatic release of glucosamine phosphate from glycogen—GP (12.5 U/ml) with or without GDE (0.5 μM) were incubated with purified glycogen (1 g/l) in 50 mM β-glycerophosphate and 10 mM KH_2PO_4, pH 7.1 in a 500 μl reaction. Reactions were incubated overnight at 25°C. Reactions were quenched by addition of an equal volume of 100% methanol. The soluble fraction, which released glucosamine phosphate, was transferred to a separate tube after centrifugation at 14,000 rpm for 10 min, dried by vacuum centrifuge at 10^{-3} mBar.

Sample derivatization—Dried polar and glycogen samples were derivatized by the addition of 20 mg/mL methoxyamine hydrochloride in pyridine and incubation for 1.5 hr at 30°C. Sequential addition of N-methyl-trimethylsilyl-trifluoroacetamide (MSTFA) followed with an incubation time of 30 min at 37°C with thorough mixing between addition of solvents. The mixture was then transferred to a v-shaped amber glass chromatography vial.

GCMS quantification—An Agilent 7800B gas-chromatography (GC) coupled to a 7010A triple quadrupole mass spectrometry detector equipped with a high-efficiency source was used for this study. GCMS protocols were similar to those described previously (Sun et al.; Young et al., 2020). Briefly, 1-μL sample aliquot was injected onto a VF-5 ms column (30 m × 250 μm internal diameter, 0.25 μm film thickness) in a 1:10 split mode. Helium gas flow rate was set at 1.5 mL/min. The temperature of the transfer line to mass spectrometer was set to 280 °C and that of the ion source was set to 220 °C. The EI energy was set to 70 eV. The modified temperature gradient was used for GC: Initial temperature was 130°C, held for 4 min, rising at 6°C/min to 243°C, rising at 60°C/min to 280°C, held for 2 min. Scan (m/z: 50 – 800) and full scan mode were used for target metabolite analysis. Metabolite EI fragmentation pattern and retention time were determined by ultrapure standard purchased from sigma. Ions (m/z) and retention time (min) used for metabolites are as follows:

Glucose (160 or 319m/z; 17.4min)

Glucosamine (159 or 319m/z; 17.6min)

Glucose 2-phosphate (387m/z, 21.1min)

Glucose 3-phosphate (387m/z 21.3min)

Glucose 6-phosphate (387m/z; 21.6min)

Glucosamine 1-phosphate (305m/z; 16.62min)

UDP-GlcNAc/GlcNAc (319mz; 19.2min)

UDP-GlcNAc/GlcNAc share the same retention due to the loss of UDP in the GC oven. We assume no free GlcNAc in the polar fraction, and no bound UDP-GlcNAc in the N-glycans. Quantification was performed using the software Mnova, Mestrelab with a primary ion and at least two or more matching qualifying ions. Relative abundance was corrected for recovery using the L-norvaline standard and adjusted to protein input (Andres et al., 2020b).

Iodine staining for glycogen chain length—Purified glycogen (50 μg in 20 μL water) was diluted with 180 μL saturated $CaCl_2$ containing 1 g/L KI and 0.1 g/L I_2, according to a previously established method (Krisman, 1962). Following incubation at room temperature for 5 min, an absorbance spectrum from 350 – 700 nm was measured. Values were normalized to the absorbance at 400 nm.

Glycogen chain length determination by high performance anionic exchange chromatography (HPAEC)—The skeletal muscle glycogen of male and female Gde KO mice was purified by the KOH procedure followed by 3 ethanol precipitation and quantified as previously described (Tagliabracci et al., 2008). Briefly, 50 μg was treated with 25 μg/ml isoamylase in 100 μL of 100 mM NaOAc pH 4.8. After Incubation at 42°C overnight, the reaction was boiled for 5 minutes, cooled to room temperature, and centrifuged at 14,000*g* to pellet any denatured protein. The supernatant was collected and 400 μL water was added. The sample was filtered through a spin filter (Costar SpinX) and loaded onto a Dionex ICS3000 HPAEC for chain length analysis using pulsed amperometric detection as previously described (Irimia et al., 2015).

Stable isotope tracing of hexosamine pathway *in vitro*—Control and shPygb primary astrocytes were maintained in DMEM supplemented with 10 mM glucose, 2 mM Gln, 10% heat-inactivated FBS in 10 cm dishes. For the tracer experiment, astrocytes (~ 50% confluency) were cultured in DMEM base media supplemented with 10 mM $^{13}C_6$-glucose, 2 mM Gln, 10% dialyzed fetal bovine serum, for 24 h in a CO_2 incubator maintained at 37 °C. At the end of incubation, cells were washed with cold PBS three times followed by extraction with acetonitrile/water/chloroform (V/V 2:1.5:1) to obtain polar metabolites for mass spectrometry analysis.

UDP-GlcNAc analysis by mass spectrometry—Polar fractions were reconstituted in 30 μL nanopure water, and analyzed on a Dionex ICS-5000+ion chromatograph interfaced to an Orbitrap Fusion Tribrid mass spectrometer (Thermo Fisher Scientific, San Jose, CA, USA) operating at a resolution setting of 500,000 (FWHM at m/z 200) on MS1 acquisition to capture any and all ^{13}C isotopologues. The Orbitrap Fusion was tuned and calibrated according to the manufacturer's default standard recommendations, to routinely achieve a mass accuracy of 0.5 ppm or better. The chromatograph was outfitted with a Dionex IonPac AG11-HC-4 μm RFIC&HPIC guard (2 × 50 mm) guard column upstream of a Dionex IonPac AS11-HC-4 μm RFIC&HPIC (2 × 250 mm) column. An m/z range of 80–700 except for the organ extracts where the m/z range was 50-750. Peak areas were integrated and exported to Excel via the TraceFinder 3.3 (Themo) software package. Peak areas were corrected for natural abundance distribution of each of the isotopologues, after which fractional enrichment were calculated to quantify ^{13}C incorporation into UDP-GlcNAc.

Formalin fixed paraffin-embedded slide preparation for MALDI-imaging— Tissues were sectioned at 4 μm and mounted on positively charged glass slides for MALDI imaging based on previous described method (Stanback et al., 2021). Brains from male and female LKO mice treated with VAL-0417 or PBS via intracerebroventricular infusion were obtained from a previous experiment demonstrating PGB clearance by periodic Schiff staining (Brewer et al., 2019). The slides were heated at 60°C for 1 hr. After cooling, tissue sections were deparaffinized by washing twice in xylene (3 min each). Tissue sections were then rehydrated by submerging the slide twice in 100% ethanol (1 min each), once in 95% ethanol (1 min), once in 70% ethanol (1 min), and twice in water (3 min each). Following the wash, the slide was transferred to a coplin mailer containing the citraconic anhydride buffer for antigen retrieval and the mailer was placed in a vegetable steamer for 25 min. Citraconic anhydride (Thermo) buffer was prepared by adding 25 mL citraconic anhydride in 50 mL water and adjusted to pH 3 with HCl. After allowing the buffer to cool, the buffer was exchanged with water five times by pouring out 90% of the buffer and replacing with water, prior to replacing completely with water on the last time. The slide was then desiccated prior to enzymatic digestion. Tris buffer pH 9 – 10 was also effective, but citraconic anhydride buffer was used for all experiments in this study.

Glycogen and N-glycan MALDI mass spectrometry imaging—An HTX spray station (HTX) was used to coat the slide with a 0.2 mL aqueous solution of either isoamylase (4 Units/slide), PNGase F (20 mg total/ slide), or both. The spray nozzle was heated to 45°C and the spray velocity was 900 m/min. Following application of PNGase F, slides were incubated at 37°C for 2 hr in a humidified chamber, then dried in a desiccator prior to matrix application [α-cyano-4-hydroxycinnamic acid matrix (0.021 g CHCA in 3 mL 50% acetonitrile/50% water and 12 μL TFA) applied with HTX sprayer]. For the detection and separation of glycogen and N-glycans, a Waters SynaptG2-Xs high-definition mass spectrometer equipped with traveling wave ion mobility was used. The laser was operating at 1000 Hz with an energy of 200 AU and spot size of 50 μm, mass range is set at 500 – 3000m/z. Images of glycogen and N-glycans were generated using the waters HDI software (Stanback et al., 2021). For the detection of larger glycans, ions were detected using a Solarix dual source 7T FTICR mass spectrometer (Bruker Daltonics) (m/z = 690–5000 m/z) with a SmartBeam II laser operating at 1000 Hz, a laser spot size of 75 μm. Images of differentially expressed glycans were generated to view the expression pattern of each analyte of interest using FlexImaging 4.0 software (Bruker Daltonics). Following MS analysis, data was loaded into FlexImaging Software focusing on the range m/ z = 1000 – 4000 and reduced to 0.95 ICR Reduction Noise Threshold.

Quantification and Statistical Analysis—All data were analyzed using the Kolmogorov-Smirnov test for normal distribution. All data were normally distributed and met the assumption of the used statistical approaches. Statistical analyses were carried out using GraphPad Prism. All numerical data are presented as mean ± SD except for xenograft tumor growth, which is presented as mean ± S.E. Grouped analysis was performed using two-way ANOVA. Column analysis was performed using one-way ANOVA or t-test. A *P*-value less than 0.05 was considered statistically significant. The statistical parameters for each experiment can be found in the figures and figure legends.

Supplementary Material

Refer to Web version on PubMed Central for supplementary material.

Acknowledgments

We would like to thank Dr. Yokota for providing the anti-PGB antibody, Vander Kooi and Gentry lab members for vigorous discussions regarding the work, Mrs. Dana Napier for performing immunohistochemistry on tissue slices and the Markey Cancer Center. The authors thank Nancy R. Gough (BioSerendipity, LLC) for editorial support.

Funding

This study was supported by National Institute of Health (NIH) grants R35 NS116824 and P01 NS097197 to M.S.G. NIH grant R01 AG066653, St Baldrick's Career Development Award, V-Scholar Grant, Rally Foundation Independent Investigator Grant to R.C.S., R01 DK27221 to P.J.R., and NIH 5R01AG06255002 to L.A.J. J.K.A.M. and L.R.C was supported by NIH/NCI training grant T32CA165990. This research was also supported by funding from the University of Kentucky Markey Cancer Center and the NIH-funded Biospecimen Procurement & Translational Pathology Shared Resource Facility of the University of Kentucky Markey Cancer Center P30CA177558. We also acknowledge partial support of this work through the University of Notre Dame Reisenauer Family GSD Research Fund.

References

Adeva-Andany MM, González-Lucán M, Donapetry-García C, Fernández-Fernández C, and Ameneiros-Rodríguez E (2016). Glycogen metabolism in humans. BBA Clin 5, 85–100. [PubMed: 27051594]

Andres DA, Young LE, Gentry MS, and Sun RC (2020a). Spatial profiling of gangliosides in mouse brain by mass spectrometry imaging. Journal of lipid research 61, 1537. [PubMed: 32482716]

Andres DA, Young LEA, Veeranki S, Hawkinson TR, Levitan BM, He D, Wang C, Satin J, and Sun RC (2020b). Improved workflow for mass spectrometry-based metabolomics analysis of the heart. Journal of Biological Chemistry.

Augé E, Pelegrí C, Manich G, Cabezón I, Guinovart JJ, Duran J, and Vilaplana J (2018). A strocytes and neurons produce distinct types of polyglucosan bodies in L afora disease. Glia 66, 2094–2107. [PubMed: 30152044]

Austin GL, Simmons ZR, Klier JE, Rondon A, Hodges BL, Shaffer R, Aziz NM, McKnight TR, Pauly JR, and Armstrong DD (2019). Central nervous system delivery and biodistribution analysis of an antibody–enzyme fusion for the treatment of Lafora disease. Molecular pharmaceutics 16, 3791–3801. [PubMed: 31329461]

Baba O (1993). Production of monoclonal antibody that recognizes glycogen and its application for immunohistochemistry. Kokubyo Gakkai Zasshi 60, 264–287. [PubMed: 8345245]

Baskaran S, Chikwana VM, Contreras CJ, Davis KD, Wilson WA, DePaoli-Roach AA, Roach PJ, and Hurley TD (2011). Multiple glycogen-binding sites in eukaryotic glycogen synthase are required for high catalytic efficiency toward glycogen. The Journal of biological chemistry 286, 33999–34006. [PubMed: 21835915]

Baskaran S, Roach PJ, DePaoli-Roach AA, and Hurley TD (2010). Structural basis for glucose-6-phosphate activation of glycogen synthase. Proc Natl Acad Sci U S A 107, 17563–17568. [PubMed: 20876143]

Bennett G, Di Giamberardino L, Koenig HL, and Droz B (1973). Axonal migration of protein and glycoprotein to nerve endings. II. Radioautographic analysis of the renewal of glycoproteins in nerve endings of chicken ciliary ganglion after intracerebral injection of [3H] fucose and [3H] glucosamine. Brain Research 60, 129–146. [PubMed: 4126748]

Benson DL, Schnapp LM, Shapiro L, and Huntley GW (2000). Making memories stick: cell-adhesion molecules in synaptic plasticity. Trends in cell biology 10, 473–482. [PubMed: 11050419]

Brewer MK, and Gentry MS (2019). Brain glycogen structure and its associated proteins: past, present and future. In Brain Glycogen Metabolism (Springer), pp. 17–81.

Brewer MK, Uittenbogaard A, Austin GL, Segvich DM, DePaoli-Roach A, Roach PJ, McCarthy JJ, Simmons ZR, Brandon JA, Zhou Z, et al. (2019). Targeting Pathogenic Lafora Bodies in Lafora Disease Using an Antibody-Enzyme Fusion. Cell Metabolism.

Buschiazzo A, Ugalde JE, Guerin ME, Shepard W, Ugalde RA, and Alzari PM (2004). Crystal structure of glycogen synthase: homologous enzymes catalyze glycogen synthesis and degradation. The EMBO journal 23, 3196–3205. [PubMed: 15272305]

Chikwana VM, Khanna M, Baskaran S, Tagliabracci VS, Contreras CJ, DePaoli-Roach A, Roach PJ, and Hurley TD (2013). Structural basis for 2'-phosphate incorporation into glycogen by glycogen synthase. Proc Natl Acad Sci U S A 110, 20976–20981. [PubMed: 24324135]

Choi R, Woo HI, Choe B-H, Park S, Yoon Y, Ki C-S, Lee S-Y, Kim J-W, Song J, Kim DS, et al. (2015). Application of whole exome sequencing to a rare inherited metabolic disease with neurological and gastrointestinal manifestations: A congenital disorder of glycosylation mimicking glycogen storage disease. Clinica Chimica Acta 444, 50–53.

Collaborative Computational Project (1994). The CCP4 suite: programs for protein crystallography. Acta Crystallogr D Biol Crystallogr 50, 760–763. [PubMed: 15299374]

Den Hollander N, Mulder D, Graaff R, Thorpe S, Baynes J, Smit G, and Smit A (2007). Advanced glycation end products and the absence of premature atherosclerosis in glycogen storage disease Ia. Journal of inherited metabolic disease 30, 916–923. [PubMed: 17570077]

DePaoli-Roach AA, Tagliabracci VS, Segvich DM, Meyer CM, Irimia JM, and Roach PJ (2010). Genetic depletion of the malin E3 ubiquitin ligase in mice leads to lafora bodies and the accumulation of insoluble laforin. Journal of Biological Chemistry 285, 25372–25381.

Deslauriers AM, Afkhami-Goli A, Paul AM, Bhat RK, Acharjee S, Ellestad KK, Noorbakhsh F, Michalak M, and Power C (2011). Neuroinflammation and endoplasmic reticulum stress are coregulated by crocin to prevent demyelination and neurodegeneration. The Journal of Immunology 187, 4788–4799. [PubMed: 21964030]

Dhugga KS, and Ray PM (1994). Purification of 1,3-beta-D-glucan synthase activity from pea tissue. Two polypeptides of 55 kDa and 70 kDa copurify with enzyme activity. European journal of biochemistry 220, 943–953. [PubMed: 8143748]

Duran J, Gruart A, López-Ramos JC, Delgado-García JM, and Guinovart JJ (2019). Glycogen in Astrocytes and Neurons: Physiological and Pathological Aspects. In Brain Glycogen Metabolism (Springer), pp. 311–329.

Duran J, Saez I, Gruart A, Guinovart JJ, and Delgado-García JM (2013). Impairment in long-term memory formation and learning-dependent synaptic plasticity in mice lacking glycogen synthase in the brain. Journal of Cerebral Blood Flow & Metabolism 33, 550–556. [PubMed: 23281428]

Emsley P, and Cowtan K (2004). Coot: model-building tools for molecular graphics. Acta crystallographica Section D, Biological crystallography 60, 2126–2132. [PubMed: 15572765]

Endo T (2005). Glycans and glycan-binding proteins in brain: galectin-1-induced expression of neurotrophic factors in astrocytes. Current drug targets 6, 427–436. [PubMed: 16026261]

Fosgerau K, Westergaard N, Quistorff B, Grunnet N, Kristiansen M, and Lundgren K (2000). Kinetic and functional characterization of 1, 4-dideoxy-1, 4-imino-d-arabinitol: a potent inhibitor of glycogen phosphorylase with anti-hyperglyceamic effect in ob/ob mice. Archives of biochemistry and biophysics 380, 274–284. [PubMed: 10933882]

Freeze HH, Eklund EA, Ng BG, and Patterson MC (2015). Neurological aspects of human glycosylation disorders. Annual review of neuroscience 38, 105–125.

Ganesh S, Delgado-Escueta AV, Sakamoto T, Avila MR, Machado-Salas J, Hoshii Y, Akagi T, Gomi H, Suzuki T, and Amano K (2002). Targeted disruption of the Epm2a gene causes formation of Lafora inclusion bodies, neurodegeneration, ataxia, myoclonus epilepsy and impaired behavioral response in mice. Human molecular genetics 11, 1251–1262. [PubMed: 12019206]

Garant PR (1968). Glycogen-membrane complexes within mouse striated muscle cells. The Journal of cell biology 36, 648. [PubMed: 5645553]

Gentry MS, Guinovart JJ, Minassian BA, Roach PJ, and Serratosa JM (2018). Lafora disease offers a unique window into neuronal glycogen metabolism. Journal of Biological Chemistry 293, 7117–7125.

Gusarov I, Pani B, Gautier L, Smolentseva O, Eremina S, Shamovsky I, Katkova-Zhukotskaya O, Mironov A, and Nudler E (2017). Glycogen controls Caenorhabditis elegans lifespan and resistance to oxidative stress. Nature communications 8, 1–12.

Harpur R, and Quastel J (1949). Phosphorylation of d-glucosamine by brain extracts (Nature Publishing Group).

Hayee BH, Antonopoulos A, Murphy EJ, Rahman FZ, Sewell G, Smith BN, McCartney S, Furman M, Hall G, and Bloom SL (2011). G6PC3 mutations are associated with a major defect of glycosylation: a novel mechanism for neutrophil dysfunction. Glycobiology 21, 914–924. [PubMed: 21385794]

Holian O, Dill D, and Brunngraber EG (1971). Incorporation of radioactivity of D-glucosamine-1-14C into heteropolysaccharide chains of glycoproteins in adult and developing rat brain. Archives of Biochemistry and Biophysics 142, 111–121. [PubMed: 5545472]

Huang Y, and Dodds ED (2013). Ion mobility studies of carbohydrates as group I adducts: isomer specific collisional cross section dependence on metal ion radius. Analytical chemistry 85, 9728–9735. [PubMed: 24033309]

Irimia JM, Tagliabracci VS, Meyer CM, Segvich DM, DePaoli-Roach AA, and Roach PJ (2015). Muscle glycogen remodeling and glycogen phosphate metabolism following exhaustive exercise of wild type and laforin knockout mice. Journal of Biological Chemistry 290, 22686–22698.

Iwaki T, Harnada Y, and Tateishi J (1996). Advanced glycosylation end-products and heat shock proteins accumulate in the basophilic degeneration of the myocardium and the corpora amylacea of the glia. Pathology international 46, 757–763. [PubMed: 8916145]

Johnson EC, Dammer EB, Duong DM, Ping L, Zhou M, Yin L, Higginbotham LA, Guajardo A, White B, and Troncoso JC (2020). Large-scale proteomic analysis of Alzheimer's disease brain and cerebrospinal fluid reveals early changes in energy metabolism associated with microglia and astrocyte activation. Nature Medicine, 1–12.

Kabsch W (2010). Xds. Acta Crystallogr D Biol Crystallogr 66, 125–132. [PubMed: 20124692]

Kimura T, Takamatsu J, Miyata T, Miyakawa T, and Horiuchi S (1998). Localization of identified advanced glycation end-product structures, Nε=(carboxymethyl) lysine and pentosidine, in age-related inclusions in human brains. Pathology international 48, 575–579. [PubMed: 9736403]

Kirkman B, Whelan WJ, and Bailey J (1989). The distribution of glucosamine in mammalian glycogen from different species, organs and tissues. BioFactors (Oxford, England) 2, 123–126.

Kirkman BR, and Whelan WJ (1986). Glucosamine is a normal component of liver glycogen. FEBS letters 194, 6–11. [PubMed: 3079709]

Kishnani PS, Austin SL, Arn P, Bali DS, Boney A, Case LE, Chung WK, Desai DM, El-Gharbawy A, and Haller R (2010). Glycogen storage disease type III diagnosis and management guidelines. Genetics in Medicine 12, 446–463. [PubMed: 20631546]

Kizuka Y, Kitazume S, and Taniguchi N (2017). N-glycan and Alzheimer's disease. Biochimica et Biophysica Acta (BBA)-General Subjects 1861, 2447–2454. [PubMed: 28465241]

Kleene R, and Schachner M (2004). Glycans and neural cell interactions. Nature Reviews Neuroscience 5, 195–208. [PubMed: 14976519]

Krisman CR (1962). A method for the colorimetric estimation of glycogen with iodine. Analytical biochemistry 4, 17–23. [PubMed: 14459704]

Lamerz AC, Haselhorst T, Bergfeld AK, von Itzstein M, and Gerardy-Schahn R (2006). Molecular cloning of the Leishmania major UDP-glucose pyrophosphorylase, functional characterization, and ligand binding analyses using NMR spectroscopy. The Journal of biological chemistry 281, 16314–16322. [PubMed: 16611637]

Liepkalns VA, Icard-Liepkalns C, Yates AJ, Mattison S, and Stephens RE (1983). Effects of human brain cell culture conditions on [14C] glucosamine radioactivity incorporation into gangliosides. Journal of lipid research 24, 533–540. [PubMed: 6875378]

López-González I, Viana R, Sanz P, and Ferrer I (2017). Inflammation in Lafora disease: evolution with disease progression in laforin and malin knock-out mouse models. Molecular neurobiology 54, 3119–3130. [PubMed: 27041370]

Ma X, and Stockigt J (2001). High yielding one-pot enzyme-catalyzed synthesis of UDP-glucose in gram scales. Carbohydrate research 333, 159–163. [PubMed: 11448677]

Mandl J, and Bánhegyi G (2018). The ER–Glycogen Particle–Phagophore Triangle: A Hub Connecting Glycogenolysis and Glycophagy? Pathology & Oncology Research 24, 821–826. [PubMed: 29981013]

McClain DA, Paterson AJ, Roos MD, Wei X, and Kudlow JE (1992). Glucose and glucosamine regulate growth factor gene expression in vascular smooth muscle cells. Proceedings of the National Academy of Sciences 89, 8150–8154.

Moseley HN, Lane AN, Belshoff AC, Higashi RM, and Fan TW (2011). A novel deconvolution method for modeling UDP-N-acetyl-D-glucosamine biosynthetic pathways based on 13 C mass isotopologue profiles under non-steady-state conditions. BMC biology 9, 1–16. [PubMed: 21214944]

Murshudov GN, Skubak P, Lebedev AA, Pannu NS, Steiner RA, Nicholls RA, Winn MD, Long F, and Vagin AA (2011). REFMAC5 for the refinement of macromolecular crystal structures. Acta crystallographica Section D, Biological crystallography 67, 355–367. [PubMed: 21460454]

Narimatsu Y, Joshi HJ, Nason R, Van Coillie J, Karlsson R, Sun L, Ye Z, Chen Y-H, Schjoldager KT, and Steentoft C (2019). An atlas of human glycosylation pathways enables display of the human glycome by gene engineered cells. Molecular cell 75, 394–407. e395. [PubMed: 31227230]

Ng BG, and Freeze HH (2018). Perspectives on glycosylation and its congenital disorders. Trends in Genetics 34, 466–476. [PubMed: 29606283]

Ng YS, and Turnbull DM (2016). Mitochondrial disease: genetics and management. Journal of neurology 263, 179–191. [PubMed: 26315846]

Nishimura A, Sawada S, Ushiyama I, Yamamoto Y, Nakagawa T, Tanegashima A, and Nishi K (2000). Lectin-histochemical detection of degenerative glycoconjugate deposits in human brain. Forensic science international 113, 265–269. [PubMed: 10978635]

Nitschke F, Ahonen SJ, Nitschke S, Mitra S, and Minassian BA (2018). Lafora disease—from pathogenesis to treatment strategies. Nature Reviews Neurology 14, 606–617. [PubMed: 30143794]

Nitschke F, Wang P, Schmieder P, Girard J-M, Awrey DE, Wang T, Israelian J, Zhao X, Turnbull J, and Heydenreich M (2013). Hyperphosphorylation of glucosyl C6 carbons and altered structure of glycogen in the neurodegenerative epilepsy Lafora disease. Cell metabolism 17, 756–767. [PubMed: 23663739]

Olaf Prante KH, Heinz H Coenen (2007). Chemoenzymatic n.c.a synthesis of the coenzyme UDP-2-deoxy-2-[18F]fluoro-α-D-glucopyranose as substrate of glycosyltransferases. Journal of labelled compounds and radiopharmaceuticals 50, 55–63.

Ondruskova N, Honzik T, Kolarova H, Pakanova Z, Mucha J, Zeman J, and Hansikova H (2018). Aberrant apolipoprotein C-III glycosylation in glycogen storage disease type III and IX. Metabolism 82, 135–141. [PubMed: 29408683]

Ondruskova N, Honzik T, Vondrackova A, Tesarova M, Zeman J, and Hansikova H (2014). Glycogen storage disease-like phenotype with central nervous system involvement in a PGM1-CDG patient. Neuroendocrinol Lett 35, 137–141. [PubMed: 24878975]

Patterson MC (2015). Congenital disorders of N-linked glycosylation. In Rosenberg's Molecular and Genetic Basis of Neurological and Psychiatric Disease (Elsevier), pp. 673–686.

Pellerin L (2003). Lactate as a pivotal element in neuron–glia metabolic cooperation. Neurochemistry international 43, 331–338. [PubMed: 12742077]

Popov N (1985). Effects of D-galactosamine and D-glucosamine on retention performance of a brightness discrimination task in rats. Biomedica biochimica acta 44, 611–622. [PubMed: 4026816]

Powers TW, Jones EE, Betesh LR, Romano PR, Gao P, Copland JA, Mehta AS, and Drake RR (2013). Matrix assisted laser desorption ionization imaging mass spectrometry workflow for spatial profiling analysis of N-linked glycan expression in tissues. Analytical chemistry 85, 9799–9806. [PubMed: 24050758]

Ramirez G (1974). Nonspecific incorporation of glucosamine into rat brain synaptosomes and endoplasmic reticulum. Biochimica et Biophysica Acta (BBA)-General Subjects 338, 337–344.

Roach PJ, Depaoli-Roach AA, Hurley TD, and Tagliabracci VS (2012). Glycogen and its metabolism: some new developments and old themes. Biochemical Journal 441, 763–787.

Roe JH, Bailey J, Gray RR, and Robinson JN (1961). Complete removal of glycogen from tissues by extraction with cold trichloroacetic acid solution. Journal of Biological Chemistry 236, 1244–1246.

Rubio-Villena C, Viana R, Bonet J, Garcia-Gimeno MA, Casado M, Heredia M, and Sanz P (2018). Astrocytes: new players in progressive myoclonus epilepsy of Lafora type. Human molecular genetics 27, 1290–1300. [PubMed: 29408991]

Sakai M, Austin J, Witmer F, and Trueb L (1969). Studies of corpora amylacea: I. Isolation and preliminary characterization by chemical and histochemical techniques. Archives of neurology 21, 526–544. [PubMed: 5344361]

Schwarz F, and Aebi M (2011). Mechanisms and principles of N-linked protein glycosylation. Current opinion in structural biology 21, 576–582. [PubMed: 21978957]

Sinadinos C, Valles-Ortega J, Boulan L, Solsona E, Tevy MF, Marquez M, Duran J, Lopez-Iglesias C, Calbó J, Blasco E, et al. (2014). Neuronal glycogen synthesis contributes to physiological aging. Aging Cell 13, 935–945. [PubMed: 25059425]

Stam F, and Roukema P (1973). Histochemical and biochemical aspects of corpora amylacea. Acta neuropathologica 25, 95–102. [PubMed: 4727741]

Stanback AE, Conroy LR, Young LEA, Hawkinson TR, Markussen KH, Clarke HA, Allison DB, and Sun RC (2021). Regional N-Glycan and Lipid Analysis from Tissues Using MALDI-Mass Spectrometry Imaging. Star Protocols *In Press*.

Stanley P, Taniguchi N, and Aebi M (2017). N-glycans. In Essentials of Glycobiology [Internet] 3rd edition (Cold Spring Harbor Laboratory Press).

Stapleton D, Nelson C, Parsawar K, Flores-Opazo M, McClain D, and Parker G (2013). The 3T3-L1 adipocyte glycogen proteome. Proteome science 11, 11. [PubMed: 23521774]

Stapleton D, Nelson C, Parsawar K, McClain D, Gilbert-Wilson R, Barker E, Rudd B, Brown K, Hendrix W, and O'Donnell P (2010). Analysis of hepatic glycogen-associated proteins. Proteomics 10, 2320–2329. [PubMed: 20391537]

Sun RC, Dukhande VV, Zhou Z, Young LE, Emanuelle S, Brainson CF, and Gentry MS (2019). Nuclear glycogenolysis modulates histone acetylation in human non-small cell lung cancers. Cell metabolism 30, 903–916. e907. [PubMed: 31523006]

Sun RC, Dukhande VV, Zhou Z, Young LEA, Emanuelle S, Brainson CF, and Gentry MS Nuclear Glycogenolysis Modulates Histone Acetylation in Human Non-Small Cell Lung Cancers. Cell Metabolism.

Sun RC, Fan TWM, Deng P, Higashi RM, Lane AN, Le A-T, Scott TL, Sun Q, Warmoes MO, and Yang Y (2017). Noninvasive liquid diet delivery of stable isotopes into mouse models for deep metabolic network tracing. Nature Communications 8, 1646.

Tagliabracci VS, Girard JM, Segvich D, Meyer C, Turnbull J, Zhao X, Minassian BA, DePaoli-Roach AA, and Roach PJ (2008). Abnormal metabolism of glycogen phosphate as a cause for Lafora disease. Journal of Biological Chemistry 283, 33816–33825.

Tagliabracci VS, Turnbull J, Wang W, Girard J-M, Zhao X, Skurat AV, Delgado-Escueta AV, Minassian BA, DePaoli-Roach AA, and Roach PJ (2007). Laforin is a glycogen phosphatase, deficiency of which leads to elevated phosphorylation of glycogen in vivo. Proceedings of the National Academy of Sciences 104, 19262–19266.

Tan C, Peterson N, and Raghupathy E (1977a). Characteristics of D-glucosamine uptake by rat brain synaptosomes. Journal of Neurochemistry 29, 261–265. [PubMed: 886332]

Tan C, Peterson N, and Raghupathy E (1977b). D-glucosamine uptake by rat brain synaptosomes. Biochimica et Biophysica Acta (BBA)-Biomembranes 464, 459–462. [PubMed: 831805]

Tomiya N, Ailor E, Lawrence SM, Betenbaugh MJ, and Lee YC (2001). Determination of nucleotides and sugar nucleotides involved in protein glycosylation by high-performance anion-exchange chromatography: sugar nucleotide contents in cultured insect cells and mammalian cells. Analytical biochemistry 293, 129–137. [PubMed: 11373089]

Wallace AC, Laskowski RA, and Thornton JM (1995). LIGPLOT: a program to generate schematic diagrams of protein-ligand interactions. Protein engineering 8, 127–134. [PubMed: 7630882]

Walls AB, Bak LK, Sonnewald U, Schousboe A, and Waagepetersen HS (2014). Metabolic Mapping of Astrocytes and Neurons in Culture Using Stable Isotopes and Gas Chromatography-Mass

Spectrometry (GC-MS). In Brain Energy Metabolism, Hirrlinger J, and Waagepetersen HS, eds. (New York, NY: Springer New York), pp. 73–105.

Wasser CR, Masiulis I, Durakoglugil MS, Lane-Donovan C, Xian X, Beffert U, Agarwala A, Hammer RE, and Herz J (2014). Differential splicing and glycosylation of Apoer2 alters synaptic plasticity and fear learning. Sci Signal 7, ra113–ra113. [PubMed: 25429077]

Winn MD, Ballard CC, Cowtan KD, Dodson EJ, Emsley P, Evans PR, Keegan RM, Krissinel EB, Leslie AG, McCoy A, et al. (2011). Overview of the CCP4 suite and current developments. Acta crystallographica Section D, Biological crystallography 67, 235–242. [PubMed: 21460441]

Worby CA, Gentry MS, and Dixon JE (2006). Laforin, a dual specificity phosphatase that dephosphorylates complex carbohydrates. Journal of Biological Chemistry 281, 30412–30418.

Yokota T, Ishihara T, Yoshida H, Takahashi M, Uchino F, and Hamanaka S (1988). Monoclonal antibody against polyglucosan isolated from the myocardium of a patient with Lafora disease. Journal of Neuropathology & Experimental Neurology 47, 572–577. [PubMed: 2845003]

Young LEA, Brizzee CO, Macedo JKA, Murphy RD, Contreras CJ, DePaoli-Roach AA, Roach PJ, Gentry MS, and Sun RC (2020). Accurate and sensitive quantitation of glucose and glucose phosphates derived from storage carbohydrates by mass spectrometry. Carbohydrate Polymers 230, 115651. [PubMed: 31887930]

Zhang H, Fillmore Brainson C, Koyama S, Redig AJ, Chen T, Li S, Gupta M, Garcia-de-Alba C, Paschini M, Herter-Sprie GS, et al. (2017). Lkb1 inactivation drives lung cancer lineage switching governed by Polycomb Repressive Complex 2. Nat Commun 8, 14922. [PubMed: 28387316]

Highlights

- Brain glycogen contains 25% glucosamine.
- A novel mass spectrometry imaging method reveals brain glycogen distributions.
- Glucosamine flux through glycogen is mediated by the enzymes GYS, GP, and GDE.
- Glycogen storage disease mutations impair protein glycosylation in the brain.

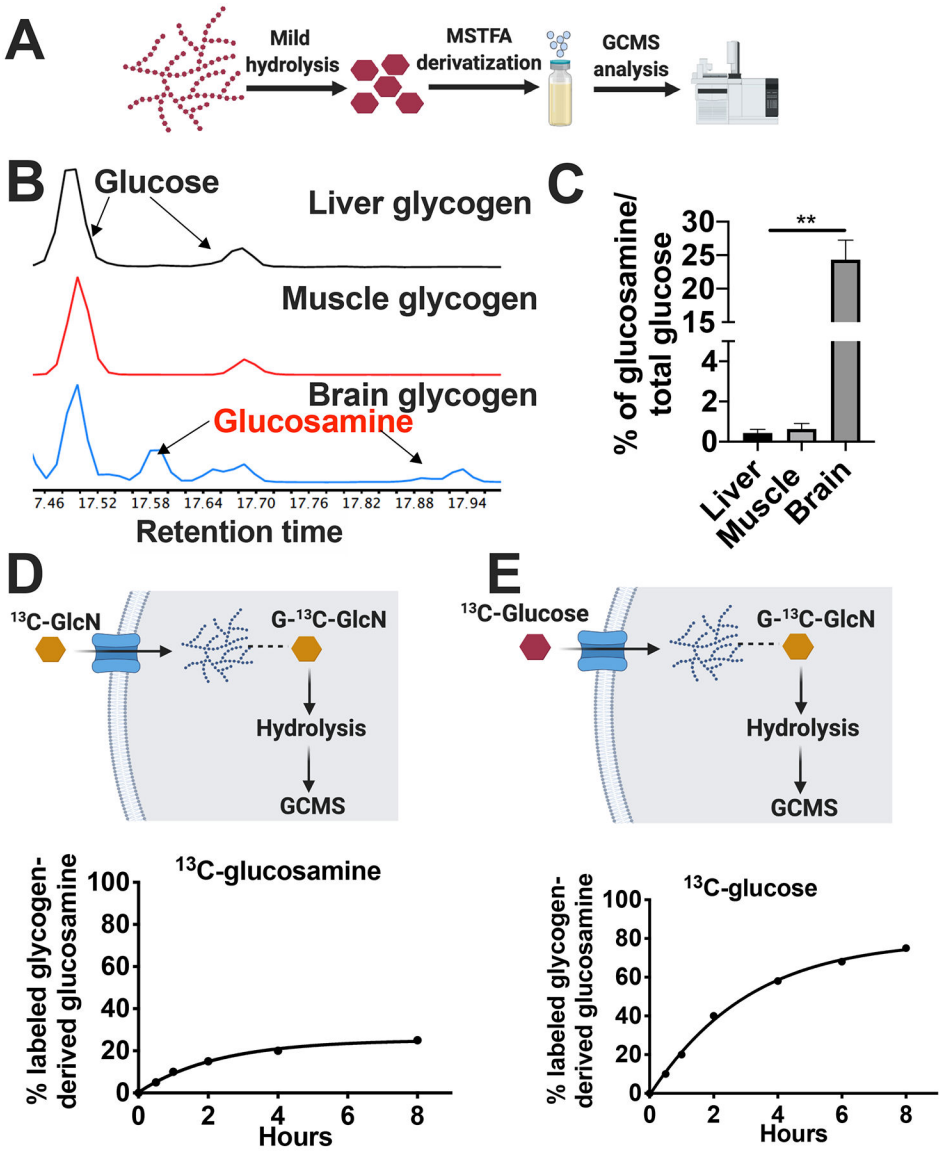

Figure 1: Glucosamine is a natural monomer of brain glycogen.

(**A**) Schematic of glycogen hydrolysis, N-methyl-trimethylsilyl-trifluoroacetamide (MSTFA) derivatization, and monomeric sugar profiling by gas chromatography mass spectrometry (GCMS).

(**B**) GCMS quantification of glucose and glucosamine in glycogen from liver, muscle, and brain with normalization to protein input.

(**C**) Glucosamine content as a fraction of total glycogen-derived glucose. Data shown are representative of three experiments and are shown as mean ± SE. ** $0.001 < P < 0.01$; two-tailed t-test.

(**D**) Top: Schematic of *in vitro* tracing of glucosamine (GlcN) incorporation into glycogen using $^{13}C_6$-glucosamine. G-^{13}C-GlcN: glycogen bound ^{13}C-GlcN. Bottom: Percent labeled glucosamine in glycogen isolated from astrocytes cultured in 2 mM ^{13}C-glucosamine for up to 8 hours. Data shown are representative of three experiments.

(**E**) Top: Schematic of *in vitro* tracing of glucosamine (GlcN) incorporation into glycogen using $^{13}C_6$-glucose. G-^{13}C-GlcN: glycogen bound ^{13}C-GlcN. Bottom: Percent labeled glucose in glycogen isolated from astrocytes cultured in 10mM ^{13}C-glucose for up to 8 hours. Data shown are representative of three experiments.
See also Figure S1.

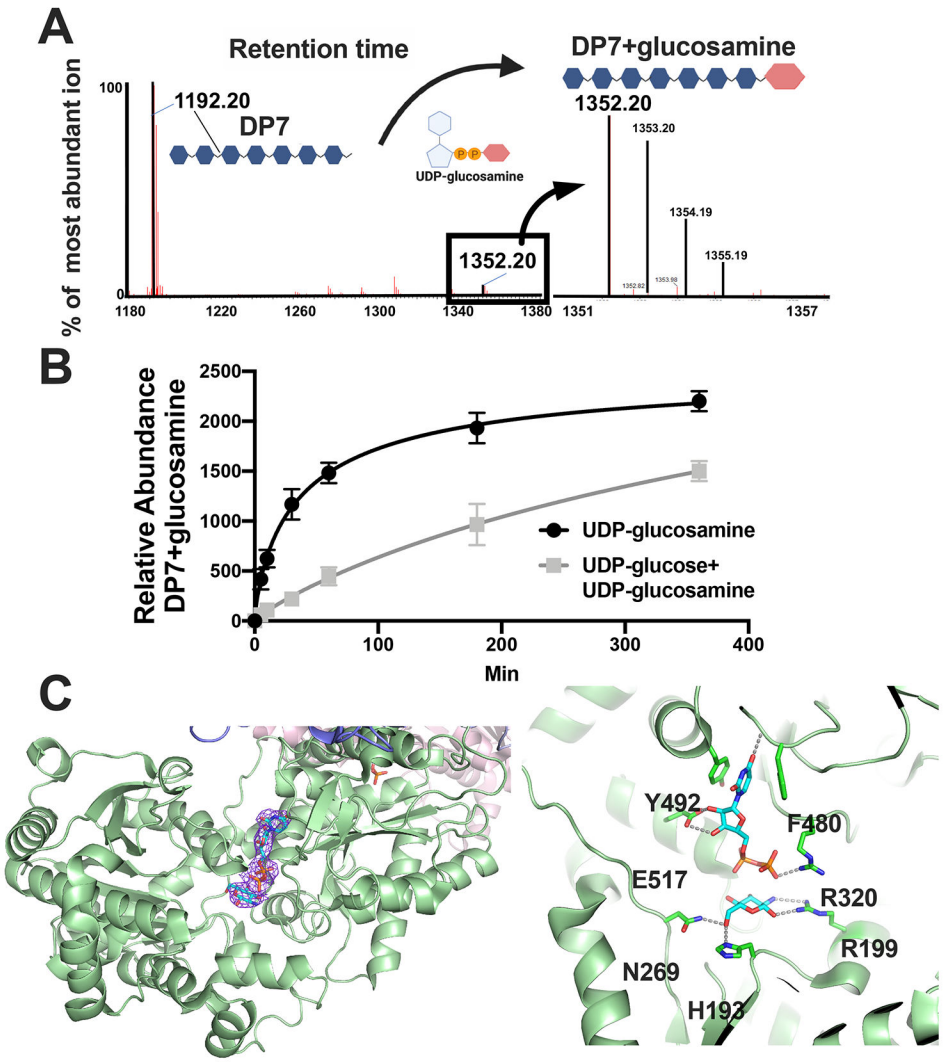

Figure 2: Glucosamine incorporation into brain glycogen by glycogen synthase.

(A) Molecular ion spectra of DP7 and DP7+glucosamine after transfer by yeast glycogen synthase (yGys). Spectra ranging from 1351 – 1357 *m/z* are enlarged to display DP7+glucosamine and its natural ^{13}C isotopologue. DP7 and DP7+glucosamine ions are highlighted. Data shown are representative of three experiments.

(**B**) Relative abundance of glucosamine transfer to DP7 over 360 min from either UDP-glucosamine (1mM) alone or UDP-glucosamine (1mM) in the presence of UDP-glucose (1mM). Data shown are representative of three experiments and are shown as mean ± SE.

(**C**) Left: Structure of UDP-glucosamine bound to the yGsy2 active site. The electron density for UDP and glucosamine is displayed (2Fo-Fc map contoured at 1σ). Right: Detailed view of the yGsy2 active site displaying the substrate-specific interacting amino acids.

See also Figure S2.

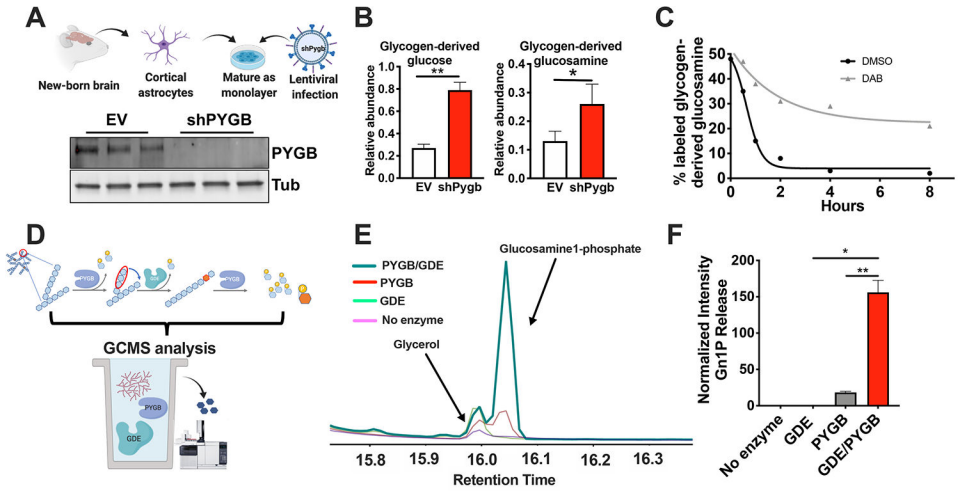

Figure 3: Glucosamine 1-phosphate release by glycogenolysis.

(**A**) Schematic of *shPygb* knockdown in primary astrocytes and immunoblot of brain glycogen phosphorylase (PYGB) in primary astrocytes after lentiviral infection with either empty vector (EV) or *shPygb*. Tubulin (Tub) serves as a loading control. Data shown are representative of three experiments.

(**B**) GCMS quantification of glucose and glucosamine from glycogen of empty vector (EV) and *shPygb* primary astrocytes.

(**C**) Turnover of glycogen-derived glucosamine in primary astrocytes. Astrocytes were cultured in 10 mM ^{13}C-glucose for 8 hours, the media was replaced with ^{12}C-glucose with either dimethyl sulfoxide (DMSO) or 1,4-dideoxy-1,4-imino-D-Arabinitol (DAB) and the percent labeled glycogen-derived glucosamine was quantified by GCMS at the indicated timepoints. Data shown are representative of three experiments.

(**D**) Schematic illustrating glycogenolysis and release of sugar phosphates by PYGB and glycogen debranching enzyme (GDE). G1P, glucose 1-phosphate (grey hexagons hexagons); Gn1P, glucosamine 1-phosphate (orange hexagons).

(**E**) GCMS quantification of released sugar phosphates from a cell-free assay with recombinant PYGB, GDE, and purified glycogen. Representative total ion chromatogram overlays of Gn1P after incubation of glycogen with the indicated enzyme combinations.

(**F**) Relative abundance of Gn1P release from enzyme combinations.

Data shown are representative of three experiments and (**B and F**) are shown as mean ± SE. *0.01 < P < 0.05; ** 0.001 < P < 0.01; two-tailed t-test.

See also Figure S3.

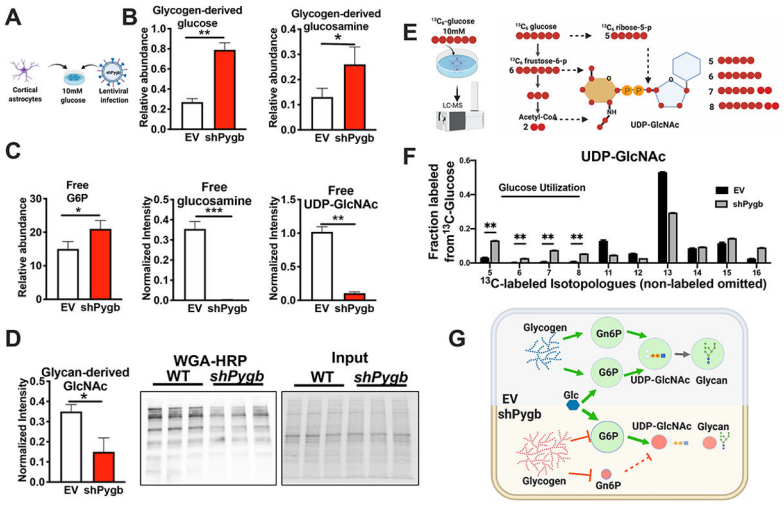

Figure 4: Aberrant glycogen metabolism reduces free UDP-GlcNAc and inhibits N-glycan production.

(**A**) Schematic of *Pygb* knockdown in primary astrocytes by lentivirus cultured in 10mM glucose.

(**B**) Relative abundance of glycogen-derived glucose and glucosamine in primary astrocytes with either empty vector (EV) or shRNA against *Pygb*. Data shown are representative of three experiments and are shown as mean ± SE.

*0.01 < P < 0.05; ** 0.001 < P < 0.01; two-tailed t-test.

(**C**) Relative abundance of free glucose 6-phosphate (G6P), glucosamine, and UDP-GlcNAc in primary astrocytes with either empty vector (EV) or shRNA against *Pygb* (shPygb). Data shown are representative of three experiments and are shown as mean ± SE.

*0.01 < P < 0.05; ** 0.001 < P < 0.01; *** P < 0.001; two-tailed t-test.

(**D**) Left: Glycan-derived GlcNAc in primary astrocytes with either empty vector (EV) or shPygb against *Pygb*. N-glycosylated proteins in EV and shPygb cultured astrocytes Wheat germ agglutinin (WGA) coupled to magnetic beads was used to precipitate glycosylated proteins, precipitated proteins were separated by SDS-PAGE and total proteins using the Bio-Rad TGX Stain-free gels were then digitally imaged. Total protein extract before the addition of WGA was used as input control. Data shown are representative of three experiments

(**E**) Schematic of isotopic tracing of $^{13}C_6$-glucose to assess hexosamine metabolism from isotopologue pattern of UDP-GlcNAc. Red circles represent possible ^{13}C labeled carbon in UDP-GlcNAc from glycolysis (fructose 6-phopshate), pentose phosphate pathway (ribose-5-phosphate), and the Krebs cycle (Acetyl-CoA). Not all possible isotopologue shown.

(**F**) Fractional labeled isotopologue distribution of UDP-GlcNAc in primary astrocytes with either empty vector (EV) or shPygb. ** 0.001 < P < 0.01; two-tailed t-test.

(**G**) Schematic of free metabolite flow between glycogen and N-linked glycans in empty vector (EV) or shPygb.

See also Figure S4.

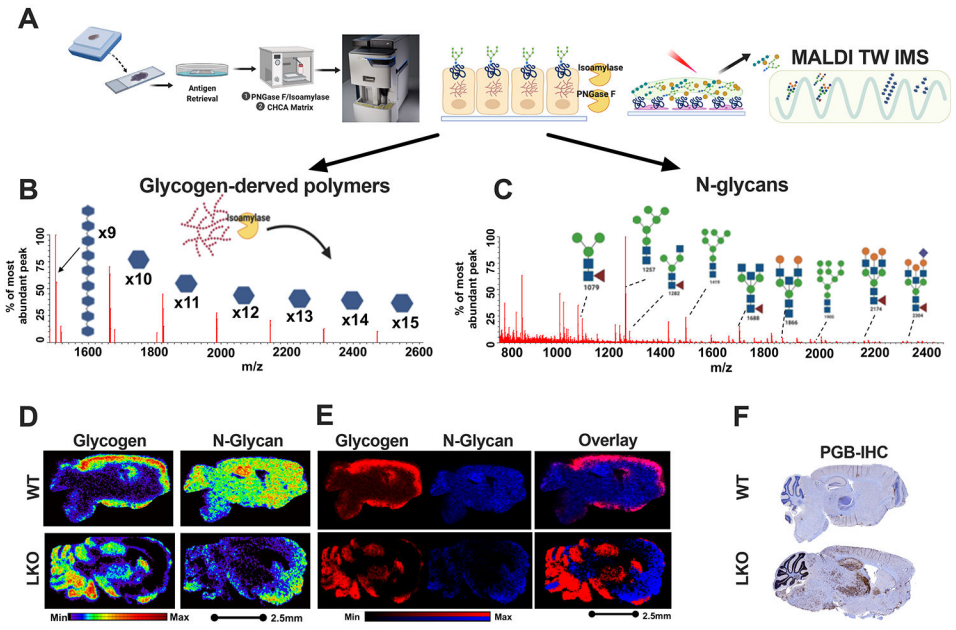

Figure 5: MALDI-mass spectrometry imaging of glycogen and N-glycans.

(A) Schematic of the workflow for dual imaging of glycogen and N-glycans. Slides are treated with peptide-N-glycosidase F (PNGase F) to release N-linked glycans, or isoamylase to cleave α-1,6-glycosidic bonds releasing linear oligosaccharide chains, or both. After adding the α-cyano-4-hydroxycinnamic acid (CHCA) ionization matrix for MALDI, samples were analyzed by MALDI and traveling wave ion mobility mass spectrometry (TW IMS).

(**B**) Representative ion chromatogram of linear polysaccharide chains derived from glycogen based on ion mobility separation. Only chain lengths of 9 – 15 are shown.

(**C**) Representative ion chromatogram of released N-glycans based on ion mobility separation, structures of the most abundant glycans are shown as diagrams.

(**D**) MALDI-MSI displaying regional and relative abundance of glycogen and N-glycans in WT and LKO mouse brain sagittal sections. Glycogen was quantified by combining linear chain polysaccharides between 4 – 15 sugar monomers long. N-glycans were quantified by combining the intensity of the three most abundant N-glycans with molecular masses of 1257, 1419, and 1688. Images display a gradient of the abundance for each.

(**E**) Images display the same data as D but presented as red for glycogen and blue for N-glycans.

(**F**) Immunohistochemical staining with an established anti-PGB antibody in WT and LKO mouse brain.

See also Figure S5.

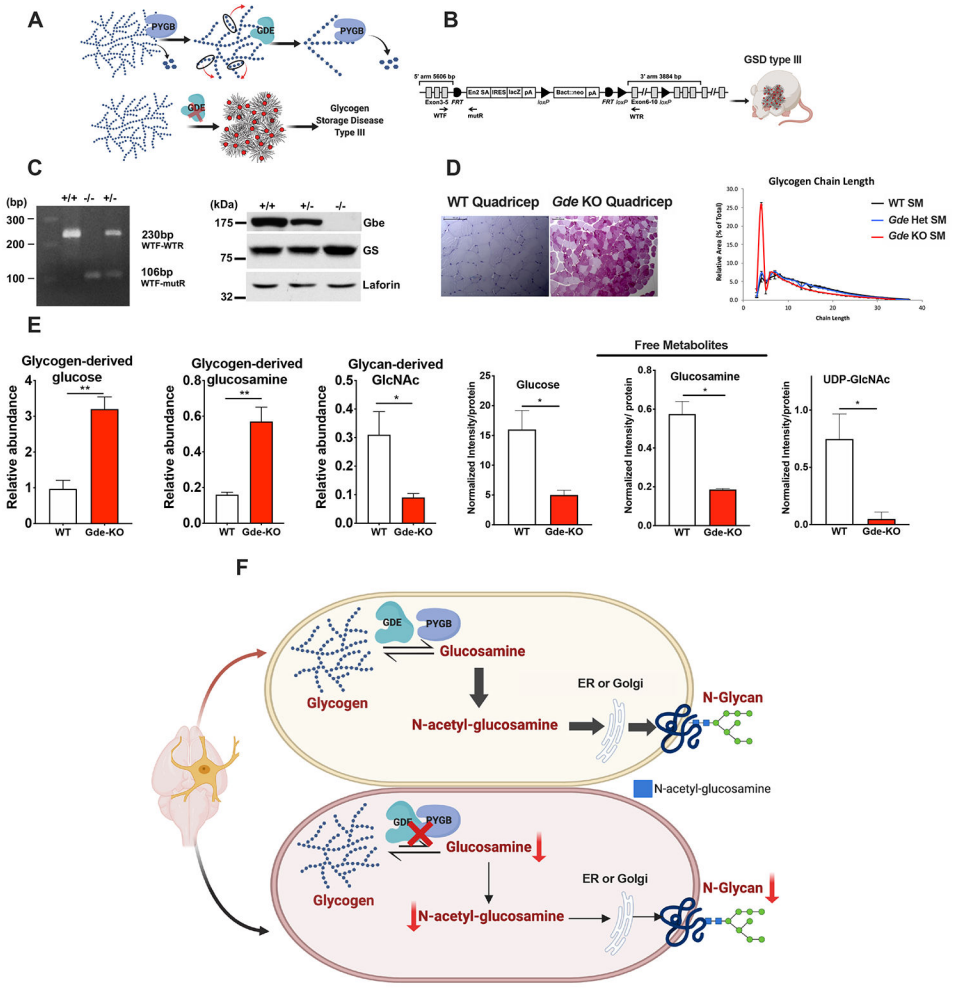

Figure 6: GSD III mouse model exhibits N-linked glycosylation defects.

(A) Schematics of glycogen degradation by glycogen phosphorylase (PYGB) and glycogen debranching enzyme (GDE) as well as glycogen storage disease III (GSD III).

(**B**) Strategy used to generate a *Gde* knockout mouse model of GSD III.

(**C**) Characterization of the *Gde* KO mouse: Confirmation of *Gde* deletion by PCR-based genotyping and Western blotting.

(**D**) Glycogen analysis in quadricep muscle from wild-type and *Gde* KO mice by Periodic acid–Schiff (PAS) staining, and glycogen chain length distribution.

(**E**) Relative abundance of glycogen-derived glucose and glucosamine, GlcNAc derived from glycan, free glucose, free glucosamine, and free UDP-GlcNAc in brains from wild-type and *Gde* KO mice. Data are shown as mean ± SE. *0.01 < P < 0.05; ** 0.001 < P < 0.01; two-tailed t-test.

(**F**) Schematic of aberrant glycogenolysis resulting in decreased N-glycan metabolism and neurodegeneration.

See also Figure S6.

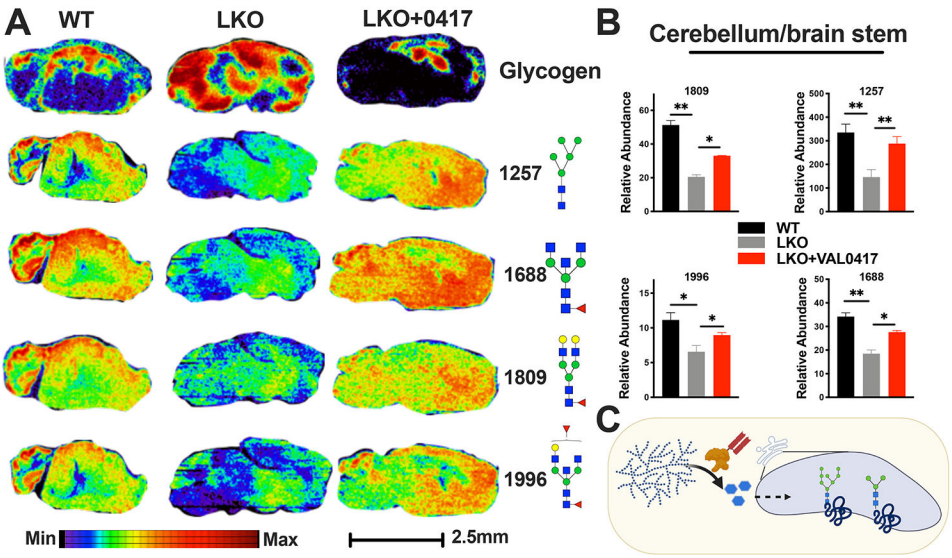

Figure 7: MALDI-mass spectrometry imaging of glycogen and N-glycans.

(**A**) MALDI-MSI displaying regional and relative abundance of glycogen and N-glycans in WT, LKO treated with PBS, and LKO treated with VAL0417 from mouse brain sagittal sections. Glycogen was quantified by combining linear chain polysaccharides between 4 – 15 sugar monomers long. Diagram of selected N-glycan structures and their *m/z* rounded to the nearest one are on the right side of the MALDI images. Images display a gradient of the abundance for each. Images shown are representative of three biological replicates.

(**B**) Relative abundance of N-glycans in WT, LKO, and LKO treated with VAL0417 quantified by total ion counts. Cerebellum and brain stem were selected for quantitation and relative abundance was normalized to total ion chromatogram (TIC) and number of pixels within in each region of interest (ROI).

Data shown are analyses of three mice and are shown as mean ± SE.

*0.01 < P < 0.05; ** 0.001 < P < 0.01; two-tailed t-test.

(**C**) Schematic of enzymatic hydrolysis of PGBs as a strategy to rescue protein hypoglycosylation.

See also Figure S7

KEY RESOURCES TABLE

REAGENT or RESOURCE	SOURCE	IDENTIFIER
Antibodies		
PYGB	LSbio	LS-B4749
GDE	Abcepta	AP2402c
hFAB™ Rhodamine Anti-Tubulin Primary Antibody	Bio-Rad	12004165
StarBright™ Blue 700 Goat Anti-Rabbit IgG	Bio-Rad	12004161
GRP78	Abcam	ab21685
GFAP	Abcam	ab7260
XBP1	Abcam	ab37152
IBA1	Abcam	ab5076
Glycogen (IV58B6)	Baba, 1993	N/A
Bacterial and virus strains		
Control shRNA Lentiviral Particles	Santa Cruz	sc-108080
PYGB shRNA (h) Lentiviral Particles	Santa Cruz	sc-105403-V
Chemicals, peptides, and recombinant proteins		
Fetal Bovine Serum	Sigma-Aldrich	F8067-500ML
DMEM (HG) With high-glucose, L-glutamine, and sodium pyruvate	Caisson Labs	DML10-6X1000ML
N-2'-O-Dibutyryl cyclic AMP (dBcAMP)	Sigma-Aldrich	DO627-250MG
Protease/Phosphatase Inhibitor Cocktail (100X)	Cell Signaling Technology	5872S
4x Laemmli Sample Buffer	Bio-Rad	1610747
Precision Plus Protein All Blue Standards	Bio-Rad	1610373
Mini-PROTEAN® TGX Stain-Free™ Protein Gels	Bio-Rad	4568024
Peroxidase conjugated wheat germ agglutinin (WGA)	Sigma-Aldrich	L3892
Clarity Max ECL HRP Substrate	Bio-Rad	1705062
U-13C6-glucose, 99%	Cambridge Isotope Laboratories	CLM-1396-MPT-PK
U-13C6-glucosamine, 99%	Cambridge Isotope Laboratories	CLM-9883-PK
1,4-dideoxy-1,4-imino-d-arabinitol (DAB)	Cayman Chemical	CAS#: 100991-92-2
UDP-Glucosamine bound yGSY2 structure	Roach Lab	PDB code: 5UW4; search model for molecular replacement was the G6P-bound yGsy2 structure (PDB code: 3NB0)
Critical commercial assays		
Pierce BCA Protein Assay Kit	Thermo Fisher Scientific	Cat. #: 23227
Liquid Diet	Harlan Laboratories	N/A
D-glucosamine-6-phosphate	Sigma-Aldrich	CAS#: 70442-23-8
FDG	Sigma-Aldrich	CAS#: 29702-43-0
Hexokinase	Sigma-Aldrich	CAS#: 9001-51-8
Phosphoglucomutase	Sigma-Aldrich	CAS#: 9001-81-4
Inorganic pyrophosphatase	Sigma-Aldrich	CAS#: 9024-82-2

REAGENT or RESOURCE	SOURCE	IDENTIFIER
Alkaline phosphatase	Sigma-Aldrich	EC#: 232-631-4
Pyruvate kinase	Sigma-Aldrich	P1506-5KU
UDP-Galactose	Sigma-Aldrich	CAS#: 137868-52-1
Maltoheptaose	CarboExpert	N/A
UDP-Glucose	Sigma-Aldrich	CAS#: 117756-22-6
a-Cyano-4-hydroxycinnamic acid	Cayman Chemical	CAS#: 28166-41-8
Trifluoroacetic acid	Sigma-Aldrich	CAS# 76-05-1
Trichloroacetic acid	Sigma-Aldrich	CAS# 76-03-9
Formaldehyde solution	Sigma-Aldrich	CAS# 50-00-0
Periodic Acid Schiff (PAS) Kit	Sigma-Aldrich	395B-1KT
Amylase	Sigma-Aldrich	CAS#: 9000-90-2
Slide-A-Lyzer	Thermo Fisher Scientific	Cat #: 88400
Trans-Blot Turbo RTA Mini 0.2 μm PVDF Transfer Kit, for 40 blots	Bio-Rad	1704274
L-Norvaline	Sigma-Aldrich	N7627-5G
Methoxyamine hydrochloride	Sigma-Aldrich	226904-25G
Pyridine	Thermo Fisher Scientific	TS-27530
MSTFA + 1 Percent TMCS	Sigma-Aldrich	375934-10X1ML
Glucose	Sigma-Aldrich	CAS#: 50-99-7
Glucosamine	Sigma-Aldrich	CAS#: 66-84-2
Glucose 2-phosphate	Roach Lab	N/A
Glucose 3-phosphate	Chiroblock	N/A
Glucose 6-phosphate	Sigma-Aldrich	CAS#: 54010-71-8
Glucosamine 1-phosphate	Sigma-Aldrich	CAS#: 2152-75-2
Isoamylase	Sigma-Aldrich	08124-5MU
Fetal Bovine Serum dialyzed	Thermo Fisher Scientific	A3382001
VAL-0417	Valerion Therapeutics	N/A
Citraconic anhydride	Thermo Fisher Scientific	CAS#: 616-02-4
PNGase F	N-Zyme Scientifics	Lot: NZL-2020-0194
Protease Inhibitor Cocktail, Roche Applied Science	Sigma-Aldrich	11697498001
Glutathione-agarose resin	Gold Biotechnology	Cat. #: G-250-5
Amicon Ultra-15 50kDA MWCO	Millipore	UFC9050
Lysozyme	Sigma-Aldrich	CAS#: 12650-88-3
Experimental models: organisms/strains		
Epm2a$^{-/-}$ mice (LKO)	Gentry Lab	N/A
Gde$^{-/-}$ (GdeKO)	MRC Harwell Institute which distributes mice on behalf of the European Mouse Mutant Archive	http://www.infrafronier.eu/; heterozygous C57BL/6N-AGLTm1aWtsi/H; Repository#EM:05784
Recombinant DNA		
pPB-His-GST-AGL protein expression plasmid	ABG Good	Cat #: 115220220300
BL21(DE3) Competent E. coli	New England BioLabs	Cat #: C2527H

REAGENT or RESOURCE	SOURCE	IDENTIFIER
Software and algorithms		
HALO Software	Indica Labs	N/A
Masslynx Software	Waters Corporation	N/A
TraceFinder 3.3	Thermo Fisher Scientific	N/A
Prism	Graphpad	N/A
HDI Software	Waters Corporation	N/A
FlexImaging 4.0 Software	Bruker Corporation	N/A
XDS Package	Kabsch, 2010	https://xds.mr.mpg.de/
MOLREP	Vagin & Teplyakov, 2010	https://scripts.iucr.org/cgi-bin/paper?dz5175
REFMAC5	Murshudov, 2011	https://www2.mrc-lmb.cam.ac.uk/groups/murshudov/
COOT	Emsley, 2010	https://www2.mrc-lmb.cam.ac.uk/personal/pemsley/coot/binaries/release/
Lipglot	Laskowski, 1996	https://www.ebi.ac.uk/thornton-srv/software/LigPlus/